UNIVERSITY OF CALIFORNIA
RIVERSIDE

Bioenergetic and Biomechanical Coupling in Sperm of the Mosquito, *Culex pipiens*

A Thesis submitted in partial satisfaction of
the requirements for the degree of

Master of Science

in

Biochemistry and Molecular Biology

by

Kaira Marie Kathryn Carstens

June 2023

Thesis Committee:

Dr. Richard Cardullo, Chairperson
Dr. Catherine Thaler
Dr. Stephanie Dingwall
Dr. Russ Hille

The Thesis of Kaira Marie Kathryn Carstens is approved:

_____

_____

_____

_____

Committee Chairperson

University of California, Riverside

Acknowledgments

I am grateful to **Dr. Richard Cardullo** for his patience, kindness, and expertise as I worked through my project. Thank you for allowing me to be independent in my experimentation while always providing guidance when needed. I could not have asked for a better PI.

I cannot understate the significance of the role **Dr. Catherine Thaler** played in my graduate education. She is one of the most knowledgeable individuals on this system and the biochemistry involved. Having the ability to discuss methods and results with her was extremely beneficial. Her attention to detail has made me a better scientist. Thank you for the countless hours you have invested in my education.

A special thank you to my lab mates, **Aly Doeve**, **Basil Alrabadi**, and **Emily Jiang**, without whom this work would not have been possible. I cannot wait to see what the future has in store for these amazing scholars!

Last, but certainly not least, I must thank **Dr. Stephanie Dingwall** for always believing in me more than I do myself. I would not have pursued a graduate level degree in biochemistry if she had not given me the opportunity to fall deeply in love with the subject. I aspire to be even somewhat close to the type of Professor, role-model, and mentor to my future students that Dr. Dingwall has been to me.

To Ronnie for all the love and support.
With you, everything is possible.

ABSTRACT OF THE THESIS

Bioenergetic and Biomechanical
Coupling in Sperm of the
Mosquito, *Culex pipiens*

by

Kaira Marie Kathryn Carstens

Master of Science, Graduate Program in Biochemistry and Molecular Biology
University of California, Riverside, June 2023
Dr. Richard Cardullo, Chairperson

Biomechanical operation of axonemal dynein requires high ATP levels; however, the source of this molecule was not yet known in sperm of the mosquito, *Culex pipiens*. Proteomics of *Culex* sperm identified glycogen phosphorylase (GP), ATP synthase beta subunit, and arginine kinase as relatively abundant. Quantifing of glycogen consumption following sperm activation by trypsin revealed increased catabolism from aerobic to anaerobic respiration. A GP inhibitor reduced glycogen consumption in a dose-dependent manor, but sperm velocity effects were complex. Glycolysis inhibition reduced velocity at all time points and extracellular glucose was not necessary until 10 minutes. Inhibition of the electron transport chain also reduced velocity at all time points without a significant difference upon extracellular glucose removal. Arginine kinase inhibition produced significant velocity reduction after 10 minutes. Additionally, extracellular calcium was confirmed to be both necessary and sufficient for sustained flagellar motility—and forward sperm velocity robustly increased at 2 minutes when 8-Br-cAMP was introduced. These results suggest trypsin activation of *Culex* sperm requires mobilization of glycogen stores for aerobic respiration providing the energy necessary for axonemal function.

Contents

List of Figures

List of Tables

Introduction

Sperm are the male gametes which, in animals, deliver a haploid set of chromosomes to a haploid ovum during fertilization that ultimately develops into a diploid organism[40]. In most taxa, sperm are motile and propel themselves through an aqueous environment to find and fertilize the ovum, using environmental cues to help them navigate their way[41]. To ensure successful fertilization, sperm must embark on this journey at the right time, on cue. In insects, sperm are made in the testes and travel through the vas deferens to a storage organ, the seminal vesicles. Here, they remain quiescent until activation is induced via mixture with accessory gland serine proteases upon ejaculation.[42, 43, 44]

Sperm quiescence during storage in the seminal vesicles is maintained by a number of environmental factors and is characterized by low cellular metabolism and little to no motility[46]. Acidity, high viscosity, high levels of calcium, and signal transduction inhibitors are examples of chemical aids to quiescence[45, 47, 48]. Additionally, some sperm are physically bound in bundles that assist with motility restriction[49]. Inhibition of motility must be accomplished in some way during storage to conserve energy stores. Upon release of inhibition, this terminally differentiated cell's phenotype, well-suited and specific for its function, allows it to initiate forward progressive motility.

Sperm are long and filamentous in order to reduce drag when moving through an aqueous environment[50]. To generate this phenotype, most of the cell's cytoplasm is extruded after spermatogenesis, and the remaining cytoplasm undergoes extensive remodeling such that a highly polarized cell is sent to the seminal vesicle for storage[10].

The head of the sperm contains the cell's haploid complement of chromosomes. In addition, in many animal sperm, a unique organelle—the acrosome—is positioned just anterior to the nucleus. The acrosome contains hydrolytic enzymes and other molecules that are thought to assist in egg recognition and penetration.[51] In *Culex*, this structure is not believed to undergo an acrosome reaction and may serve an alternative, unknown, function[52, 17]. The tail of an animal sperm ranges in length from approximately 40 μm (sea urchin)[28] to 58,000 μm[29] (*Drosophila* bifurca) and eventually tapers off to a sharp tip. The tail of *Culex* sperm is approximately 200 μm[17], slightly longer than the flagella of many mammalian sperm[30]. Within the tail lies an evolutionarily conserved structure that is essential for cellular propulsion, the axoneme.

The canonical axonemal structure is described as "9 + 2", denoting an outer circle of nine doublet microtubules with a central pair of singlet microtubules. Radial spokes connect the central pair to the outer doublets while nexin links connect neighboring doublets[31]. These components comprise the structural foundation of the axoneme. However, it is the outer and inner dynein arms that allow for the motility of the flagellum. The cytoplasmic counterparts of these motors are known for their function in cellular trafficking[32]. In the axoneme, they are attached to one set of doublets instead of carrying and eventually letting go of cargo. However, their ATPase and power stroke activities are conserved[33].

Missing or disorganized axonemes can result in immotile sperm and, therefore, infertility[7,8]. Understanding the axonemal molecular mechanisms contributing to motility activation could, therefore, be instrumental to finding strategies for male fertility

reduction. While most insect species conform to a "9 + 9 + 2" axonemal pattern consisting of nine outer singlet microtubules, nine adjacent doublets, and a central pair of singlets, *Culex* and other mosquito sperm have been observed to have a lone central singlet (Figure 1). The central rod of this "9 + 9 + 1" structure has a larger diameter and is more solid than its paired counterparts in other insect sperm.[9]

Although the axoneme's importance in motility cannot be understated, it occupies relatively little space within the flagellum of *Culex* sperm. Most of the flagellar volume is composed of mitochondrial derivatives formed by complex fusion and division events of several small mitochondria during sperm maturation. The derivatives expand outward as the flagellum develops, and eventually reach from the nuclear base to the end of the tail.[10] This is not typical of animal sperm, as many localize mitochondria to the base of the head extending outward into a fraction of the tail known as the midpiece[30]. Not only is the morphogenesis of insect sperm mitochondria unusual, but their chemical makeup is also surprising.

The most effective use of aerobic respiration requires extensive inner membrane folding into cristae to increase the surface area available for the electron transport chain (ETC) in oxidative phosphorylation. However, in place of these cristae, *Culex* sperm develop solid phase paracrystalline material composed primarily of sperm-leucylaminopeptidases (S-laps) that have lost catalytic function[10,11]. Orthologs of these proteins were abundant in the *Culex* sperm proteome[18]. The mitochondrial derivatives are believed to provide structural and elastic support to the flagellum[34], but some paracrystalline derivatives may retain partial respiratory function[35]. In the parasitic

vector *Rhodnius prolixus*, the paracrystalline material is physically connected to the axoneme at microtubule doublets one and five[24], providing a direct pathway for viscoelastic support between the axoneme and mitochondrial derivatives. Given the extensive mitochondrial modification in insect sperm flagella, it was of interest to determine the pathways used to provide bioenergetic support for motility of the axoneme, and whether aerobic respiration played a significant role in that motility.

Extensive experimentation of axonemal dynein functionality in the protist, *Chlamydomonas,* has provided insight into how the molecular motors function. Multiple dynein isoforms differing in regulatory mechanisms may exist within a single flagellum. Because the relationship between sliding velocity and ATP concentration follows Michaelis-Menten kinetics, it can be assumed that cooperativity does not exist between ATP-binding subunits or adjacent motors.[12] This independent regulation likely allows for the flagellar bending necessary for forward cellular propulsion as the nexin linkers between microtubules resist their displacement. This feature is not just a structural bridge, but has also been found to contain the dynein regulatory complex (DRC). Several other potential sites of regulation have been identified within the axoneme. Interestingly, experiments suggest the outer dynein arms are responsible for regulating flagellar beat frequency while an inner arm dynein and DRC work together to produce bending.[12] Regulation of microtubule sliding is also achieved by covalent modification. Dynein can be phosphorylated and adenylylylated, and the microtubules themselves can be polyglycosylated, polyglutamylated, tyrosinated, and acetylated. Individually, these post-translational modifications have been shown to affect flagellar motility.[12, 35, 36, 37, 38]

Additionally, the linker protein, central pair, and dynein are all capable of binding calcium or calmodulin[12]. It has been suggested that a calcium sensor (LC4) within the outer dynein arm induces the conformation necessary for microtubule-dynein interaction when two calcium molecules are bound (Figure 2)[13]. The motors take on three distinct conformations: unbound from the microtubule in an inhibitory conformation, bound to the microtubule, and unbound from the microtubule in preparation for a power stroke.[13] It is the repetition of the last two conformations which allows for microtubule sliding and subsequent flagellar motility.

Previous studies from our laboratory demonstrated that calcium is necessary for *Culex* sperm motility[17] and evidence suggests a role for a T-type calcium channel in increasing intracellular calcium[23]. The differential calcium regulation of dynein motors may allow for changes in flagellar beat patterns. Interestingly, mosquito sperm have been shown to swim backward both *in vitro* and *in vivo*[17, 27], and studies in *Culex* have shown that calcium concentrations after sperm activation dictate swimming direction[17].

Backward swimming velocities of *Drosophila* sperm *in vivo* were reported to average approximately 36 μm/sec[27], but this parameter has yet to be measured in *Culex*. Forward cellular velocities in *Culex* sperm are dependent upon waveform and vary from 5 to 75 μm/sec[17]. Regardless of direction, the cellular machinery producing waveforms capable of cellular propulsion have a high energy demand. This study aimed to uncover the metabolic pathways involved in the better-established phenomenon of forward cellular propulsion.

ATPase activity of the dynein motor is necessary for flagellar motility to generate the power stroke allowing for sliding of adjacent microtubules.[13] The major focus of this study, therefore, is to discover the source of ATP in *Culex* sperm. Due to the unusual state of the mitochondrial derivatives, the role of anaerobic pathways in motility was the first area of focus. With long, filamentous flagella such as that of *Culex* sperm, diffusion of ATP from a localized glycolytic source alone is likely not sufficient to spread energy throughout the tail. Thus, it is expected that the cell has highly strategic energy-production systems in place. One option is to utilize a flux transfer chain such as creatine kinase to propagate the displacement of ATPase activity equilibrium such that the reaction favors the production of ADP and P_i along the length of the flagellum[14]. Another potential method is an equal distribution of glycogen and glycolytic enzymes throughout the tail.

Whatever energy-production mechanisms are in place in *Culex* require regulation to switch from an inactive to active states. Because an influx of calcium alone is both necessary and sufficient for initiation of *Culex* sperm motility[23] and trypsin has been shown to effectively induce motility[17], it is likely that the trypsin receptor and T-type voltage-gated calcium channel are connected through a signal transduction pathway. The exact identities of the trypsin-activated and T-type calcium channels remain unknown, but previous studies on *Culex* sperm indicated a MAPK phosphorylation event is necessary for robust activation[17]. The presence of ERK1/2 and p38-like MAPKs in the *Culex* sperm proteome later confirmed the potential of this signaling pathway[18].

In mammals, two major activation pathways prevail: one for calcium influx and one for protein kinase A (PKA) activation[20]. These findings agree with the previously discovered necessity of calcium and a phosphorylation event in *Culex* sperm, suggesting conserved activation pathways. However, mammalian sperm, as well as sperm from many other taxa, are known to use the sperm-specific cation channel, CatSper, for calcium influx[20] and this channel is not present in insects[39]. An odorant receptor co-receptor (Orco) heteromeric ion channel has been suggested as a potential calcium influx mechanism in *Anopheles* mosquitoes[22]. However, this finding has yet to be confirmed and the channel has not been detected in *Culex* sperm. It is also not yet known how initiation of motility is coupled to an increase in catabolic activity of the cell to provide the energy necessary for propulsion.

A current hindrance to fully understand flagellar motility is the lack of consistency in methods across studies resulting in a lack of consistency in findings. With the recent invention of computer assisted sperm analysis (CASA) systems, this impedance is decreasing. While full systems are available that require specific hardware for the software system, a few open-source CASA programs are readily available online and compatible with multiple microscopy and computer operating systems likely already in place in a laboratory setting. One example of such a program is SpermQ. This program analyzes many motility parameters and the subsequent outputs can be used to investigate a wide variety of sperm motility behaviors. The software is periodically updated as users contact the creator to request additional functionality. The current study will be the first of our knowledge to use SpermQ as a method of investigating bioenergetics in sperm.

Figure 1: The "9 + 9 + 1" *Culex* axoneme with partially crystallized mitochondria

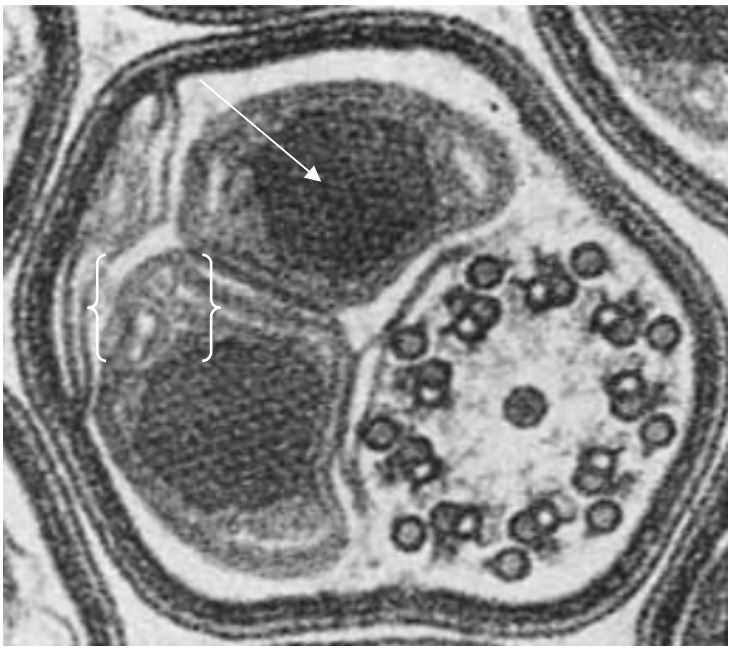

A transmission electron micrograph of a transverse section through *Culex* spermatozoa shows paracrystalline material taking up most of the mitochondrial derivative volume (arrow). However, notable folding near the mitochondrial outer membrane (brackets) is also seen. The axoneme lies adjacent to the paired derivatives and displays the non-canonical "9 + 9 + 1" axonemal pattern.

Image adapted from Phillips 1969, Figure 8[9]

Figure 2: Calcium changes dynein arm conformation to induce microtubule binding

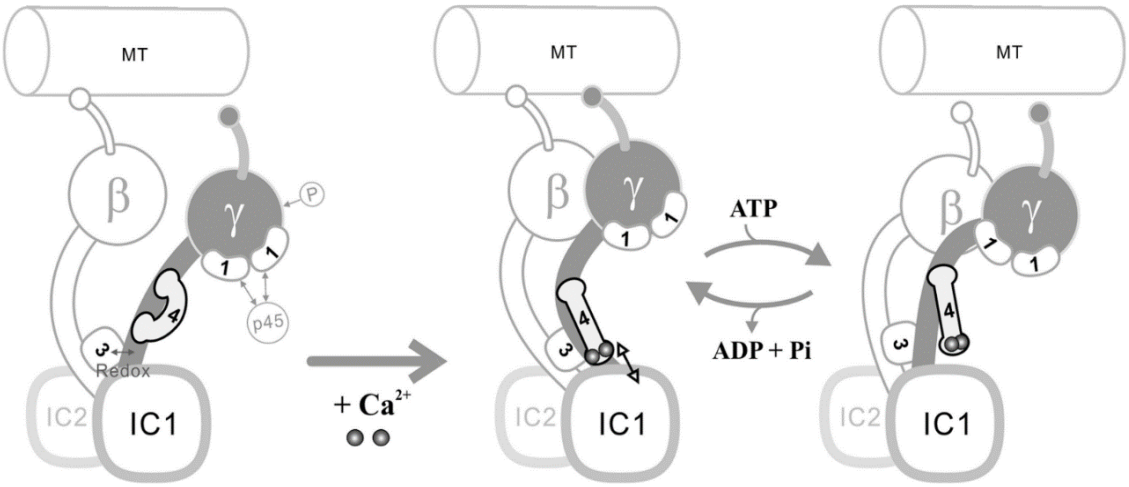

Trimeric docking complexes (DC) are necessary for beta and gamma heavy chains of dynein to bind their respective microtubule (MT). In the absence of calcium, light chain four (4) is tightly associated with the gamma heavy chain which forces it to maintain a conformation inhibiting DC-MT interaction; motility cannot be achieved if microtubule sliding is not possible. Upon calcium binding, LC4 releases its inhibition of the gamma heavy chain and associates with intermediate chain one (IC1). This allows for DC-MT interaction. ATP binding produces a bend in the gamma heavy chain such that upon its hydrolysis and ADP + P_i release, a power stroke is produced. The last two conformations then cycle producing a continuous flagellar waveform.

Image adapted from Sakato et. al. 2007, Figure 10[13]

Materials & Methods

Animals

The mosquito colony, anesthetization, and euthanasia specifics used in this study are as described in Thaler et. al. (2023) apart from males being individually isolated prior to euthanasia and experimentation.

Sperm Isolation

Culex pipiens males were obtained from cages where mating complexes could be observed. Reproductive tracts were isolated in PBS (2 mM NaH_2PO_4, 10 mM Na_2HPO_4, 135mM NaCl), then accessory glands and testes were dissected from the seminal vesicles. Seminal vesicles were washed twice with PBS prior to placement in experimental solutions. They were then squeezed between forceps to release sperm and removed from solution.

Proteomics

Three proteomic trials were completed by Thaler et. al. (2023), which are referred to as Proteomes 1 through 3 (P1-P3). Using each proteome's reported hits for each protein, a scatterplot was created to observe a rough estimate of relative abundances (Figure 3). This revealed asymptotic curves which clearly show most proteins being detected at low levels while few have significantly higher relative abundances. Where a break in the graph could be seen in the curve leading up to each proteome's asymptote, a

threshold for further investigation was created. A list of metabolic enzymes with hits greater than or equal to 50 in P1, 80 in P2, and 150 in P3 were compiled. Several aminopeptidases met these thresholds, but they were excluded due to their suspected structural role in sperm and loss of catalytic function[18]. Relative abundances were calculated with respect to the maximum number of hits detected in that respective proteome trial.

Motility Assays

Slide Setup

Slides and coverslips were cleaned with 100% ethanol. A solution depth of approximately 228.6 μm was maintained by fixing three layers of Scotch double-sided tape on the long edges of a slide and placing a coverslip over 30 μL of the appropriate solution (Figure 3). Recordings of swimming sperm were taken at the midpoint between the top of the slide and bottom of the coverslip to ensure flagellar waveforms were not affected by proximity to the glass.

Video Acquisition and Analysis

All motility assays were conducted at room temperature in Insect Ringer's (110 mM NaCl, 5 mM KCl, 0.5 mM $CaCl_2$, 1.2 mM $MgCl_2$, 1.2 mM $MgSO_4$, 1.2 mM $NaHCO_3$, 2 mM KH_2PO_4, 2 mM Na_2HPO_4, 1 mM glucose, 20 mM HEPES, pH 7.4). When possible, motility assays were conducted and analyzed in a double-blind fashion. The assays included in this group are those that were activated with 200 ng/mL of trypsin: glucose-free, calcium-free, PFK-1 inhibition,

glycogen phosphorylase inhibition, electron transport chain inhibition, anoxic solution, and arginine kinase inhibition. Adjustments to Ringer's were made as necessary (Table 1). Reagents were obtained from ThermoFisher Scientific or Sigma-Aldrich. Videos of sperm were acquired via Nikon Labophot dark field microscopy at 10x magnification. An Edgertronic camera recorded videos using the following settings: 8000 ISO, shutter speed of 1/100 seconds, frame rate of 100 per second, 1280 horizontal pixels, 1024 vertical pixels, and duration of 10 seconds. SpermQ and ImageJ software were used to analyze videos and obtain quantitative measurements of sperm phenotypes via Gaussian fit[16]. Resulting kymographs were then graded to assess data quality and those not meeting the threshold for analysis (C or higher) were excluded (Figure 4a).

Velocity Calculations

To obtain a data set most accurately reflecting the population, percent motility was calculated for each time point (Figure 4b). Nine velocity values were sought per time point (three per the three fields of view). Percent motility of nine cells gave the number of cells which should be analyzed by SpermQ for velocity versus those that should have velocity populated as zero (nonmotile). When the number of cells passing kymograph and head position in space thresholds was less than the desired number of cells to calculate velocity of, percent motility of that time point was extrapolated to a lower number. Additional trials were completed until at least twenty-seven velocity values were obtained per time point.

Head coordinate positions (x,y,t) obtained from SpermQ analysis were used to construct scatterplots of swimming sperm trajectories. Because the parameter of interest is forward cellular velocity, not the velocity at which the head of the sperm moves, the cell was treated as a cylinder whose forward trajectory could be described by the linear trendline of the head coordinate graph. The equation of the line was used to calculate the start and endpoint of a cell's "midpoint" (Figure 4b). The distance between these points divided by the time of travel was used to estimate velocity. In cases where linear trendlines did not accurately represent sperm trajectories, the actual start and endpoints were used to calculate velocity if the line between them was generally parallel to the cell's line of trajectory. In cases where kymograph grading resulted in an F but the software's tracking of the head was accurate as visualized by the "Head position in space" graph output (i.e. a clear path from one point to another without gaps in tracking was observed), the head coordinate positions were included in the data set. Additionally, in cases where kymographs were graded as meeting the threshold but there were gaps in the head position tracking or sporadic points out of order of the trend, these erroneous points were excluded from the data set (Figure 2c). Due to the nature of these calculations, the values obtained are expected to be estimates of forward cellular velocity and not representative of how fast the cell truly moves through its waveform. However, the estimates are a proper parameter for comparison of forward cellular velocity between assay conditions.

Statistical Analyses

Error bars in graphs represent the standard error of the mean. Significance between groups was calculated using 2-way ANOVA and least squares means differences student's t-test calculators in JMP 16 Pro ($\alpha = 0.05$).

Glycogen Assays

Glycogen Assay kits were obtained from Cell Bio-Labs (MET-5022). Assays were conducted in 96-well plates and analyzed with an Epoch plate reader via Gen5 1.11 software. A standard curve was used to estimate glycogen concentration per 50 µL of solution. Hemocytometry was used to estimate cell concentration in each condition. Assay conditions are as described in Table 1.

Figures

Figures were created in BioRender and Microsoft Excel.

Figure 3: Motility assay slide setup

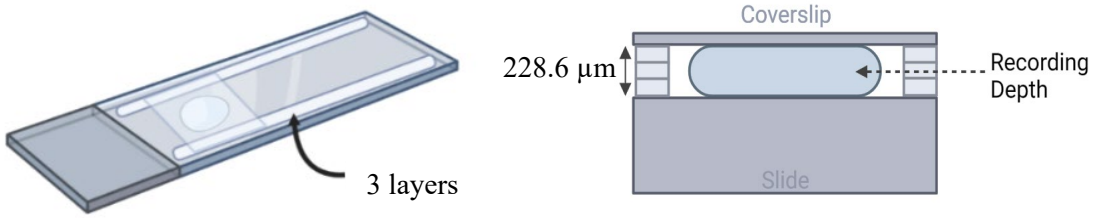

Microscopy slides were prepared with 3 layers of double-sided tape affixed to their long edges. With a thickness of 76.2 µm each, a swimming depth of 228.6 µm was created for the sperm. Recordings were taken at a depth of approximately 114.3 µm.

Figure 4: Velocity calculations

Figure 4a – Kymograph grading system

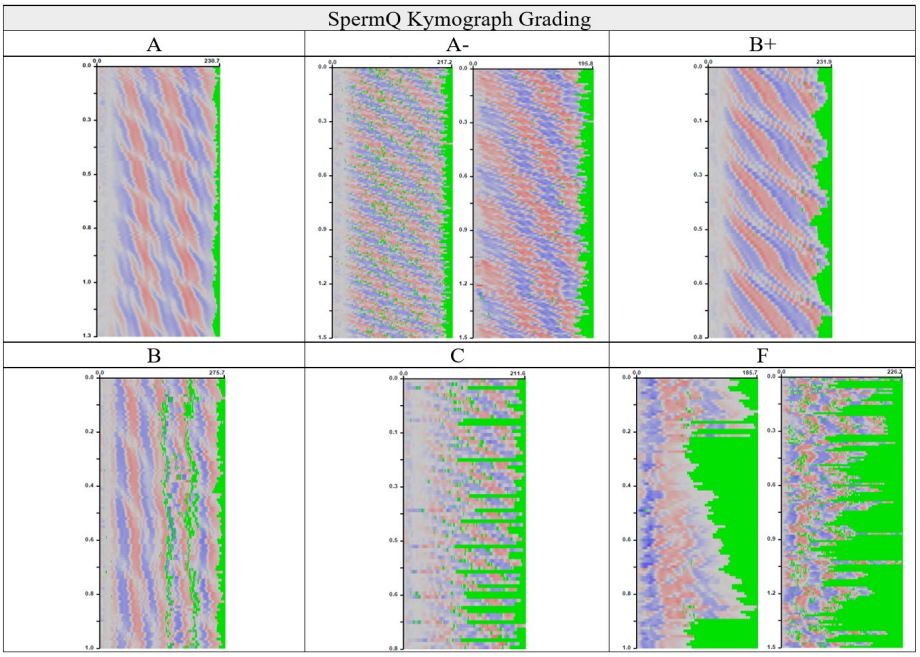

Kymograph outputs from SpermQ[16] provide a useful tool for data quality evaluation. The horizontal axis represents each position along the flagellum while the vertical axis represents time. Waveform generation over time can then be observed from the top to bottom of each graph. Areas of green indicate positions where the software was unable to track the flagellum. High ratings (B or higher) of these outputs are of the utmost importance when analyzing flagellar beat frequency and amplitude, but lower ratings (down to F) are acceptable when only head tracking is desired for velocity calculations.

Figure 4b – Using percent motility in velocity calculations

$$Percent\ Motility = \frac{\#\ Motile\ Cells}{\#\ Motile\ Cells\ +\ \#\ Nonmotile\ Cells} \times\ 100\%$$

$$Number\ of\ cells\ to\ calculate\ velocity\ of\ = \left(\frac{\%\ Motility}{100}\right) \times\ 9$$

Percent motility was calculated out of 9 cells per time point when possible. Total cell number was lowered when necessary.

Figure 4c – Using head coordinate positions to calculate velocity

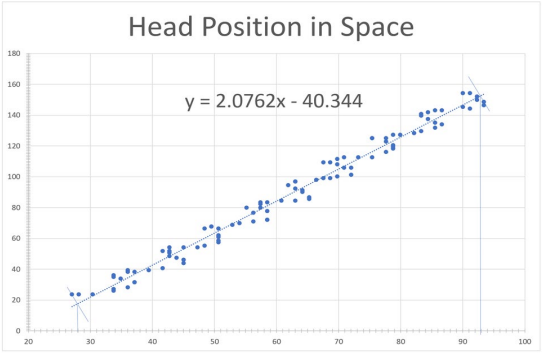

Plotting the head coordinate positions and obtaining a line of best fit allows for distance calculations. Values where the endpoints land on the x or y axis (depending on the cell's trajectory) are then used in the line of best fit to find their counterpart on the y or x axis, respectively.

Figure 4d – Excluding erroneous points from the data set

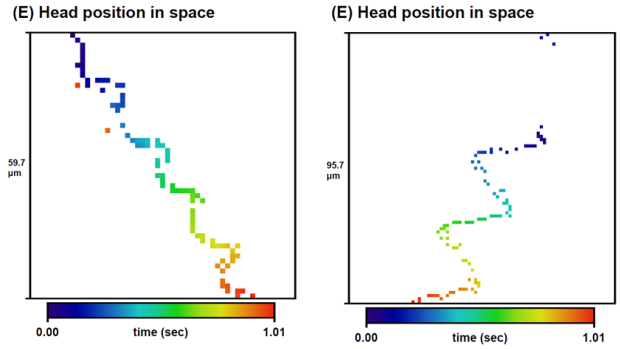

When erroneous points were obtained due to software tracking issues, they were manually deleted from the dataset using the SpermQ Head position in space output graph[16] as a guide.

Table 1: Assay chemicals

Condition	Working Concentration	Alterations to Ringer's
Glucose-Free	0 mM Glucose	1 mM Mannitol
Calcium-Free	0 mM Calcium ($CaCl_2$)	1.0 mM EGTA
PFK-1 Inhibition	5 or 10 mM Citric Acid	pH adjustment as needed
Glycogen Phosphorylase Inhibition	2, 5, 20, 50, or 200 nM Glycogen Phosphorylase Inhibitor (GPI)	1% DMSO
Electron Transport Chain Inhibition	5 mM Potassium Cyanide	Reduce KCl by 5 mM
Glucose-Free Electron Transport Chain Inhibition	0 mM Glucose 5 mM Potassium Cyanide	1 mM Mannitol Reduce KCl by 5 mM
Anoxic Solution	1 mM Sodium Dithionite	Reduce NaCl by 1 mM
Arginine Kinase Inhibition	10 mM Sodium Nitrate	Reduce NaCl by 10 mM
Orco Activation	0.1 mM VUAA1	1% DMSO
Protein Kinase A Activation	10 mM 8-Br-cAMP (Sodium Salt)	Reduce NaCl by 10 mM
DMSO Control	1% DMSO	

Chemicals and their concentrations used for motility and glycogen assays are provided. Alterations made to Ringer's, if any, are indicated.

Results

Proteomics

The *Culex pipiens* sperm proteome was instrumental in creating a metabolic enzyme profile for the cell such that subsequent metabolic activation and or inhibition experiments could be specific to the cell's enzymatic repertoire. Whole proteome abundances are reported in Figure 5. Proteomes 1 and 2 both returned arginine kinase as significantly abundant. Proteome 3 had two additional proteins not present in the other trials: glycogen phosphorylase and ATP synthase beta subunit. Relative abundances of these enzymes are reported in Table 2. In all cases, abundances were highest in the third proteome.

All enzymes included in the main steps of glycolysis, fermentation, and glycogen metabolism were searched for. This often required searching for enzymes by several different terms due to variability in biochemistry terminology. The relative abundances of each enzyme were calculated as described above (Table 3). This information was used to create graphics of anaerobic metabolic pathways with respect to enzymatic abundances (Figure 6).

Glycogen Assays

The calcium-free Ringer's (CFR) condition was analyzed to mimic quiescence in sperm and estimate the amount of glycogen stored prior to activation. The results suggest approximately 1.7 nM glycogen was stored per cell. The 1x Ringer's (1XR) condition tested the amount of glycogen consumed when sperm spontaneously activate. After

incubation in Ringer's for 40 minutes, sperm reduced glycogen stores to an average of 1.0 nM per cell. The 1XR plus trypsin (1XR+T) condition estimated the amount of glycogen consumed when sperm were fully activated into motility by a serine protease. After 40 minutes of robust activation, sperm contained only 0.5 nM glycogen per cell. Lastly, Ringer's with KCN and trypsin but without glucose (KCN-Glc+T) was used to investigate anaerobic glycogen consumption in the absence of glucose. Upon inhibition of the electron transport chain, sperm had only 0.4 nM glycogen left per cell after 40 minutes. (Figure 7a) Glycogen consumption across conditions is reported in Table 4.

The GPI's published IC_{50} is 53 nM for human liver glycogen phosphorylase[21], but was unknown for the *Culex* sperm isoform and so a dose response curve was created to aid in future studies. Plotting the concentration of GPI vs that of glycogen remaining per cell after 40 minutes of incubation indicated a hyperbolic relationship on a linear scale (Figure 7b) and sigmoidal on a semilog scale (Figure 7c). With 200 nM GPI, an average of 2.0 nM glycogen remained per cell. When only DMSO was added to Ringer's, 0.6 nM glycogen remained in each cell after incubation. The 20 nM condition was excluded from the dataset as it was an obvious outlier from both trends.

Motility Assays

Double-Blind

The control condition, trypsin-activated sperm (1XR+T), was included to provide a positive control as well as a threshold for activation with which to compare other conditions. The calcium-free condition (CFR) was included as a

negative control to confirm that, even in a double-blind setting, calcium is necessary for motility. In the control condition, a maximum average velocity of 67 μm/sec was seen at 2 minutes. This parameter reduced to 41 μm/sec at 10 minutes. In the CFR, sperm never displayed forward cellular velocity. (Figure 8a)

A glycogen phosphorylase inhibitor (GPI) was used to investigate the necessity of glycogen catabolism for forward progressive motility. The prediction was that motility would drastically reduce when the threshold for glycogen phosphorylase inhibition was met. Both 5 and 50 nM GPI were significantly effective in decreasing velocity. (Figure 8b)

A glucose-free (Glc-free) condition allowed for the investigation of the requirement of extracellular glucose for motility. Mannitol was included to replace the osmolarity lost from glucose exclusion. The predicted outcome was that sperm motility would not be affected because of the cell's glycogen storage capability. However, a slight but significant decrease in velocity occurred at minute 10. (Figure 8c)

Citric acid was used to inhibit phosphofructokinase 1 (PFK1)[57], the committed step of glycolysis. Although this molecule is not membrane-permeant, a multi-specific organic anion transporter on the plasma membrane (CpipJ_CPIJ011958)[18] has been shown to permeate citrate in other systems[25]. With the pH of Ringer's adjusted to 7.4 after the addition of citric acid, it was ensured that the dominant form of this species would be citrate in solution (pKa values = 3.1, 4.7, and 6.4). Because the IC_{50} of the enzyme was not known for this

system but was expected to be between 0 and 10 mM[58], 5 and 10 mM concentrations were chosen for experimentation. The predicted outcome was robust inhibition of motility upon meeting the threshold for PFK1 inhibition. A reduction in velocity was seen at each time point in both concentrations ($p < 0.05$) with no significant difference between them. (Figure 8d)

KCN was introduced as a first attempt at discerning the mitochondrial ETC's role in motility. To maintain the resting plasma membrane potential, a necessity for the proper function of voltage-gated channels, KCl was replaced by KCN. The ETC was again inhibited but in the absence of extracellular glucose (KCN-Glc). The aim was to establish whether glycogen catabolism was mainly anaerobic or also aerobic via the oxidation of NADH from glycolysis at the ETC. The prediction remained consistent between KCN conditions in that motility was not expected to be significantly reduced due to the mitochondrial paracrystalline material. Surprisingly, robust inhibition was observed in both cases with no significant difference between treatments. (Figure 8e)

To generally test the necessity of aerobic respiration, sodium dithionite was added to scavenge oxygen in the solution and provide an anoxic environment. NaCl was reduced accordingly to maintain sodium gradients across the plasma membrane. It was predicted that a slight decrease in motility would be observed due to the harsh nature of dithionite, but that a significant reduction would not be seen due to the mitochondrial derivatives. This was true at 2 minutes, but a significant decrease in velocity was observed at minutes 6 and 10. (Figure 8f)

Because the proteome uncovered the cell's high abundance of arginine kinase (both cytosolic and membrane-bound) and its known role as an ATP shuttle system in other insects, sodium nitrate was used to inhibit such a potential system[56]. NaCl was again reduced to maintain sodium gradients. It was predicted that if this system assists in the transport of ATP along the length of the flagellum or regeneration of ATP at the axoneme, then its inhibition will decrease motility, and potentially only at certain regions along the flagellar length (most likely the distal end). Significant inhibition of motility was seen at 10 minutes. (Figure 8g)

Orco Activation

In an attempt to reproduce Pitts' 2014 activation of mosquito sperm via Orco stimulation[22], VUAA1 was used as a replacement for trypsin. It was predicted that if Orco was part of a signaling pathway initiating flagellar motility, the introduction of a known Orco activator would induce forward cellular progression. Moderate activation was observed with a significant difference between VUAA1-activated and trypsin-activated motility at 2 minutes ($p < 0.05$) but not at 6 or 10 minutes. Due to the necessity of DMSO for this hydrophobic chemical, two vehicle controls were conducted to ensure its introduction to Ringer's did not alter motility on its own. There was no significant difference between Ringer's and Ringer's with DMSO. (Figure 9)

Protein Kinase A Activation

Due to the regulatory signal transduction pathway of glycogen phosphorylase[26], it was predicted that protein kinase A activation via a membrane-permeable cAMP derivative (8-Br-cAMP) would induce flagellar motility without the addition of trypsin. Extremely robust flagellar activation was seen at 2 minutes with an average velocity reaching 97.5 μm/sec. Interestingly, this enhanced motility was lost by 6 minutes. (Figure 10)

Average velocities across all motility assay conditions are listed in Table 5. Conditions are ranked by velocity in descending order according to the 10-minute time point. A total of 139 trials were run to obtain velocity values for 2229 cells.

Figure 5: *Culex* sperm protein abundances

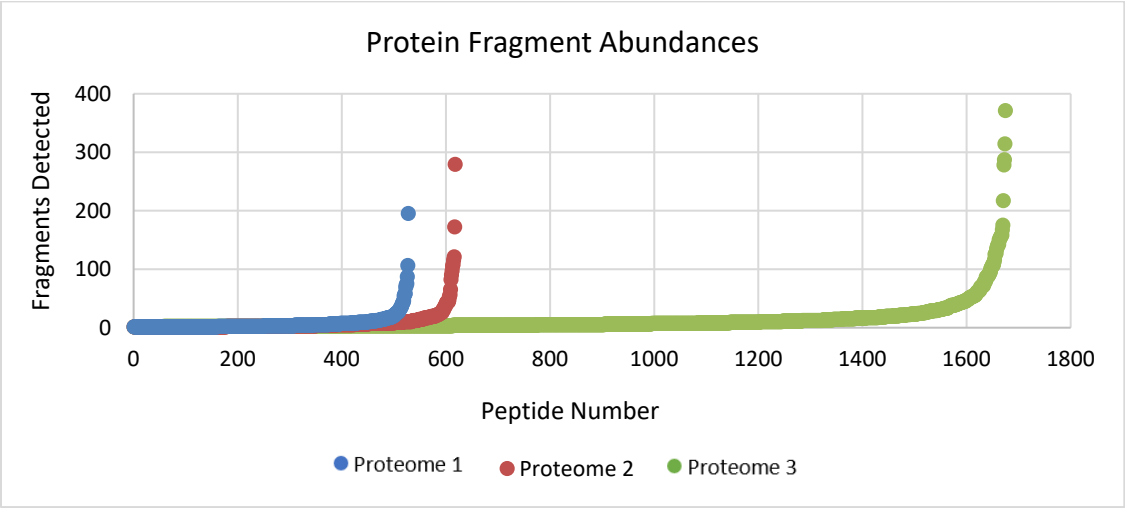

A scatterplot of the number of fragments detected for each unique peptide in the three proteomes was used to visualize the position and shape of the curve leading into the asymptote. Thresholds were chosen around the midpoint of the curve where a gap could be seen upon zooming in.

Data obtained from Thaler et. al. 2023[18]

Figure 6: Anaerobic metabolic pathways of *Culex pipiens* sperm

Figure 6a: Glycolysis and lactic acid fermentation

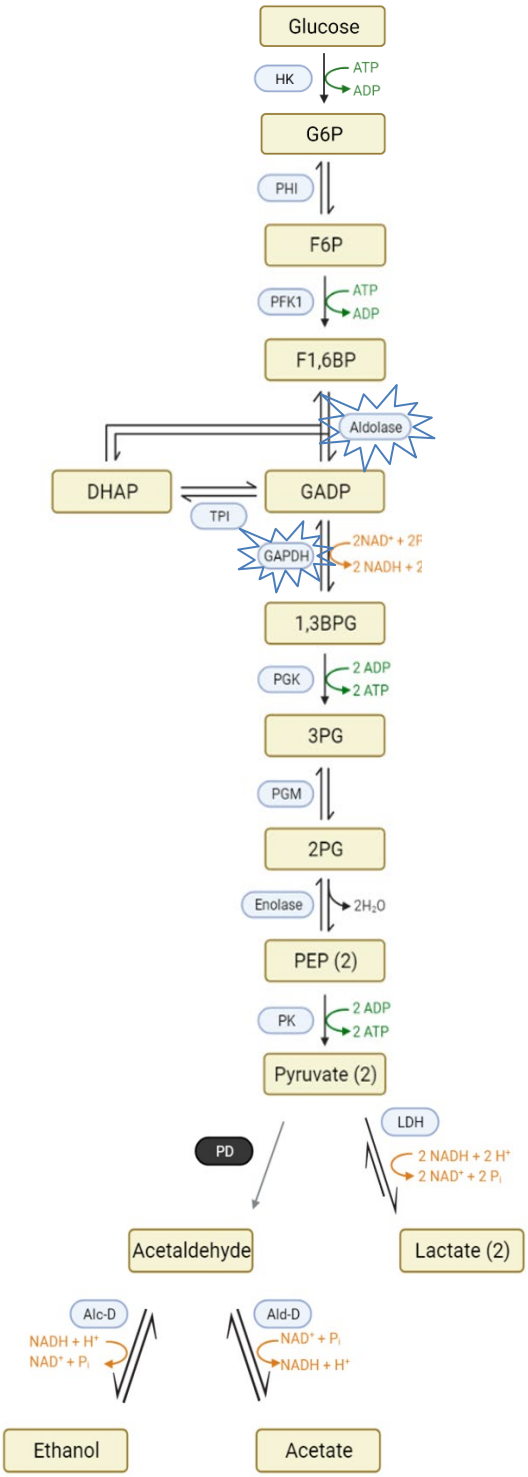

Figure 6b: Glycogen metabolism

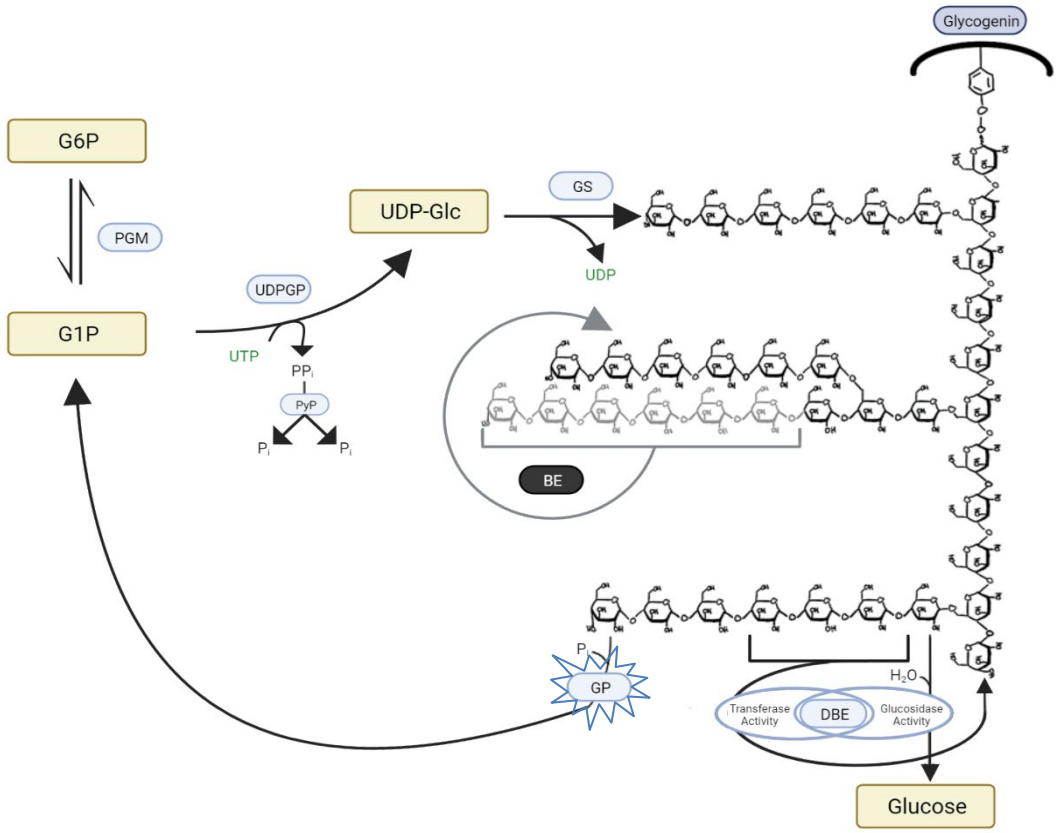

Figure 6a: Glycolytic enzymes and intermediates are shown leading into lactic acid fermentation.

Figure 6b: Glycogenic enzymes and intermediates are shown.

Enzymes which were not found in the proteome and molecules subsequently not known to be involved in the pathway are blacked out. Enzymes with relative abundances greater than or equal to 25% in Proteome 3 of Table 3 are emphasized to visualize the steps of the pathway which are upregulated by the cell.

Figure 7: Glycogen concentrations

Figure 7a: Glycogen across conditions

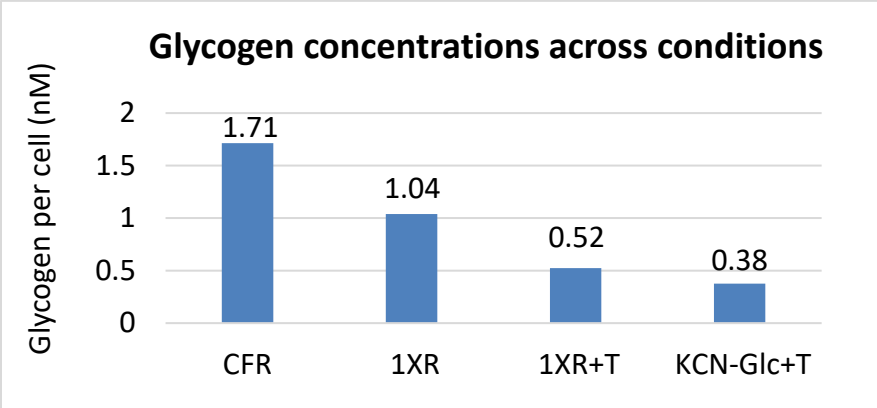

Glycogen decreased from mimicked quiescence to spontaneous activation to induced activation to induced activation with ETC inhibition without glucose, respectively.

Figure 7b: Linear GPI dose response

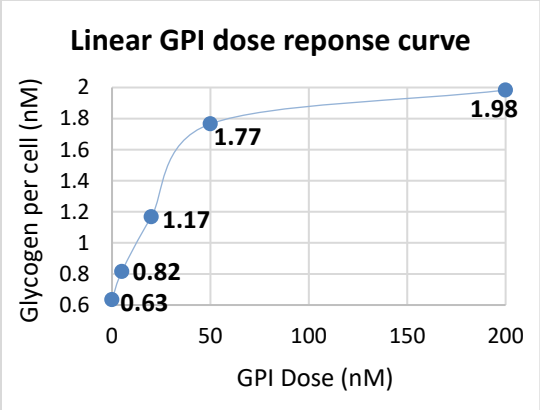

Figure 7c: Semilog GPI dose response

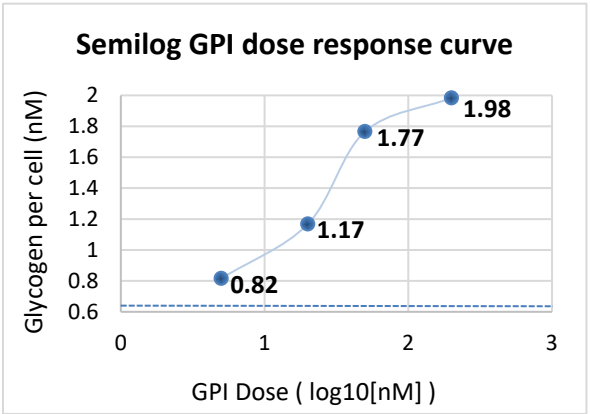

Figure 7b: GPI inhibition of glycogen phosphorylase follows a hyperbolic curve when graphed on a linear scale.

Figure 7c: GPI inhibition of glycogen phosphorylase follows a sigmoidal curve when graphed on a semilog scale. The dotted line indicates where GPI = 0 nM would lie.

Figure 8: Velocity across conditions

Figure 8a: Positive and negative control velocities

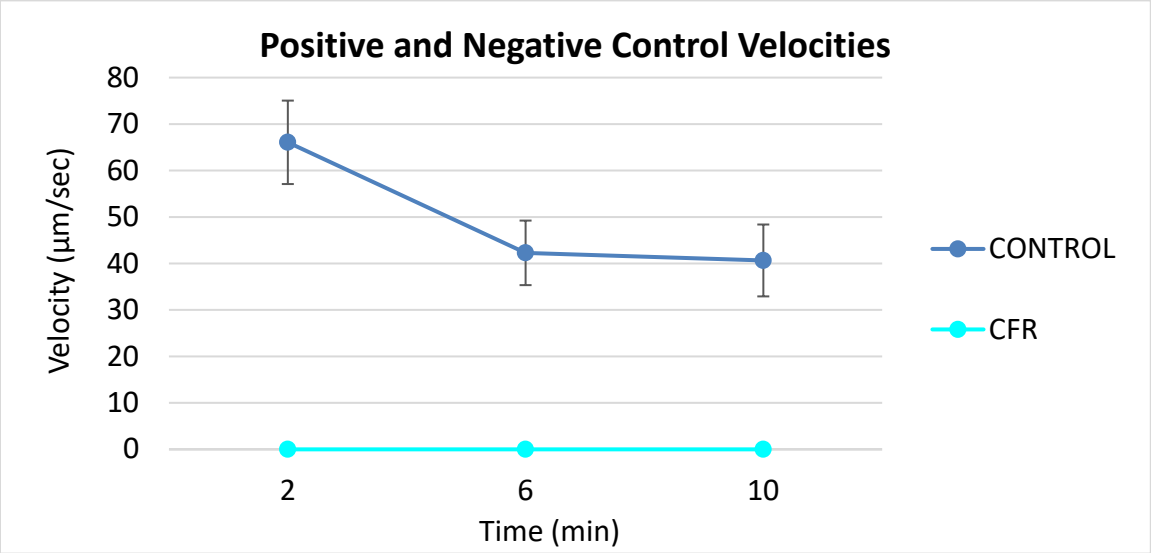

Control velocities began at an average of 66 µm/sec 2 minutes post activation with trypsin. Forward progression decreased significantly to 42 µm/sec at 6 minutes ($p < 0.05$) and remained constant with an average of 40 µm/sec at 10 minutes. Sperm in calcium-free Ringer's never attained forward cellular velocity.

Figure 8b: Velocity under glycogen phosphorylase inhibition

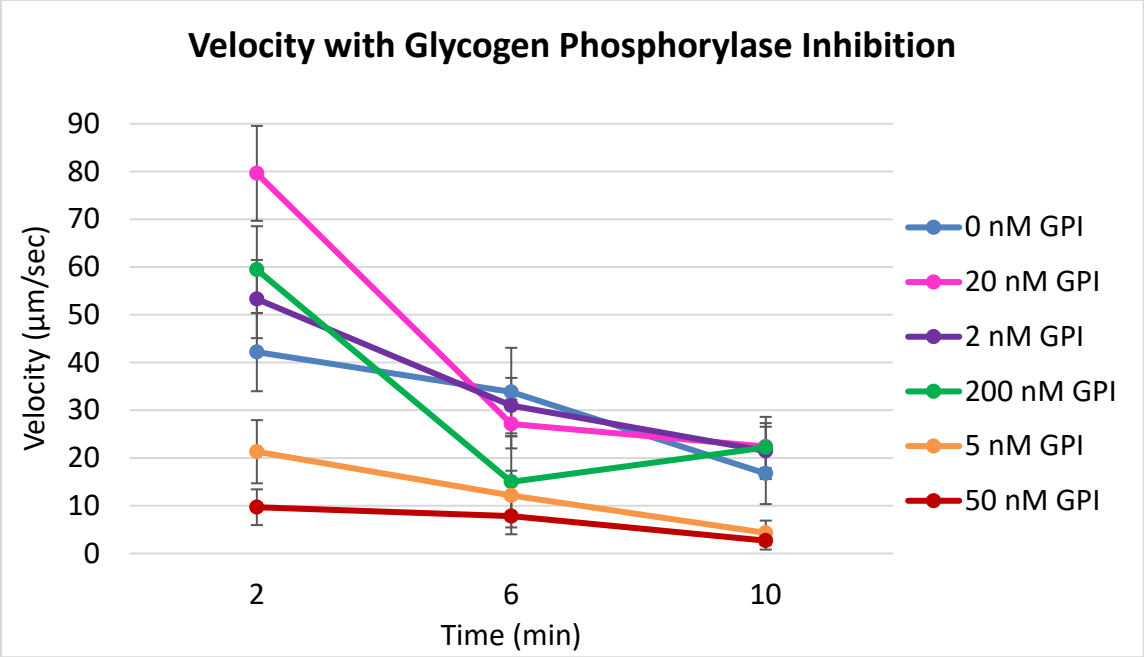

A comparison of average velocities over time shows no difference between 5 and 50 nM GPI as they both significantly reduce velocity at 2*, 6**, and 10*** minutes (*$p < 0.0001$, **$p < 0.05$, *** $p < 0.0001$). Significant inhibition is also seen at 6 minutes in 200 nM GPI ($p < 0.05$). Interestingly, 2, 5, and 200 nM conditions produced significantly increased velocities at minute 10 ($p < 0.05$).

Figure 8c: Velocity in glucose-free Ringer's

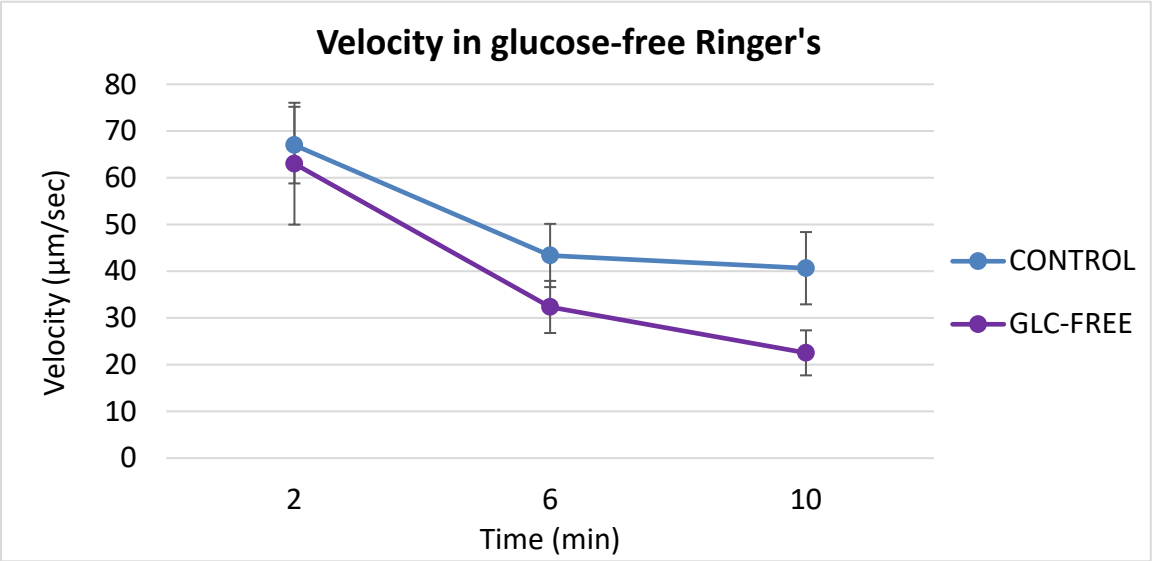

Removing glucose from the extracellular space caused velocity to decrease slightly. The most significant difference is seen at minute 10 ($p < 0.05$).

Figure 8d: Velocity under PFK1 inhibition

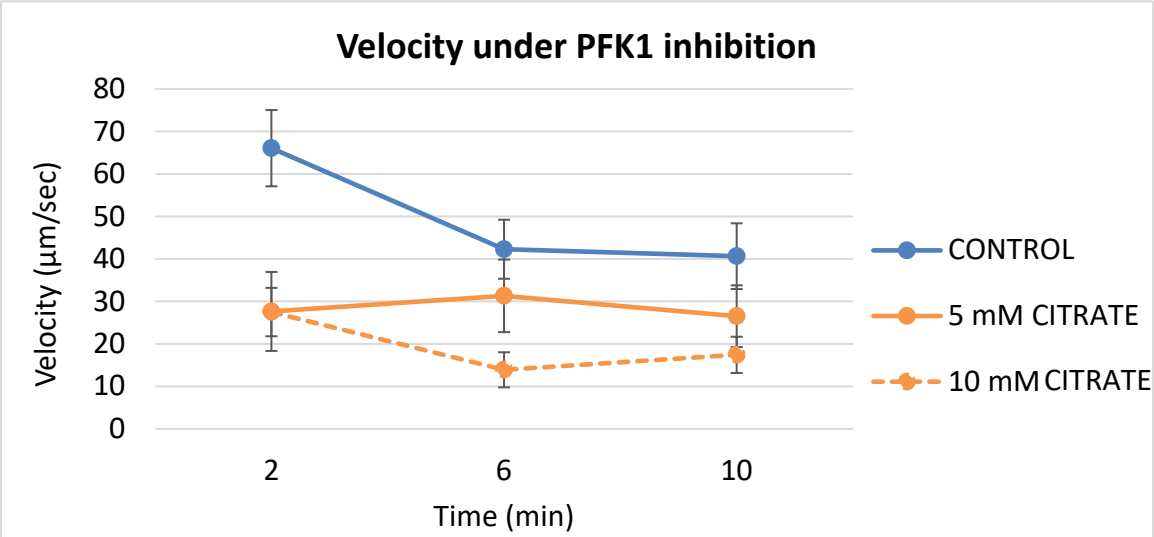

Velocity decreased in Ringer's containing 5 or 10 mM citrate. Robust inhibition was seen at 2 minutes where both concentrations significantly reduced velocity with respect to control ($p < 0.0001$). This decreased velocity remained relatively constant.

Figure 8e: Velocity under ETC inhibition with and without glucose

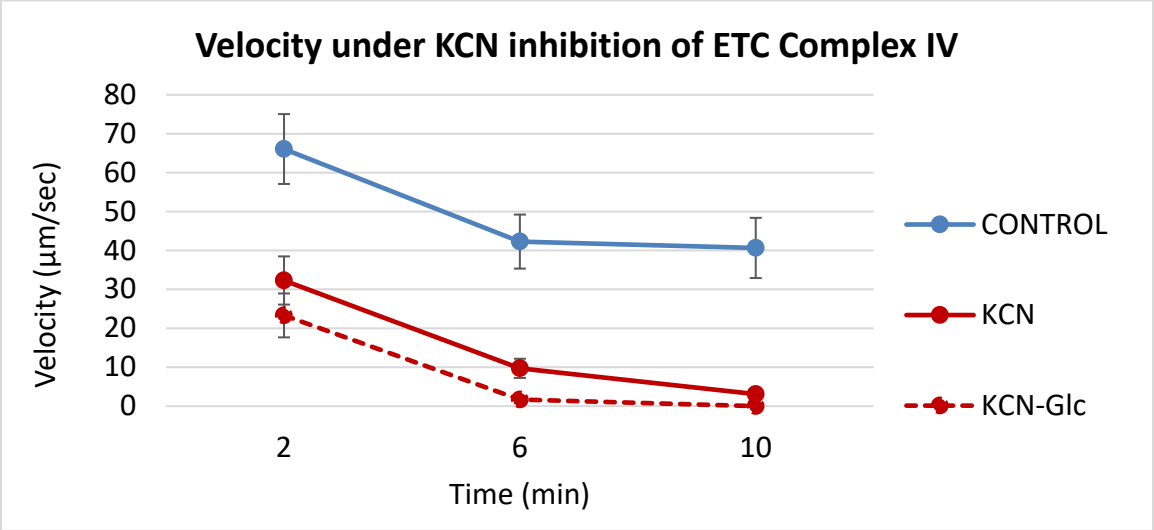

Velocity is seen to be significantly reduced in both anaerobic conditions ($p < 0.0001$).

Figure 8f: Velocity in anoxic conditions

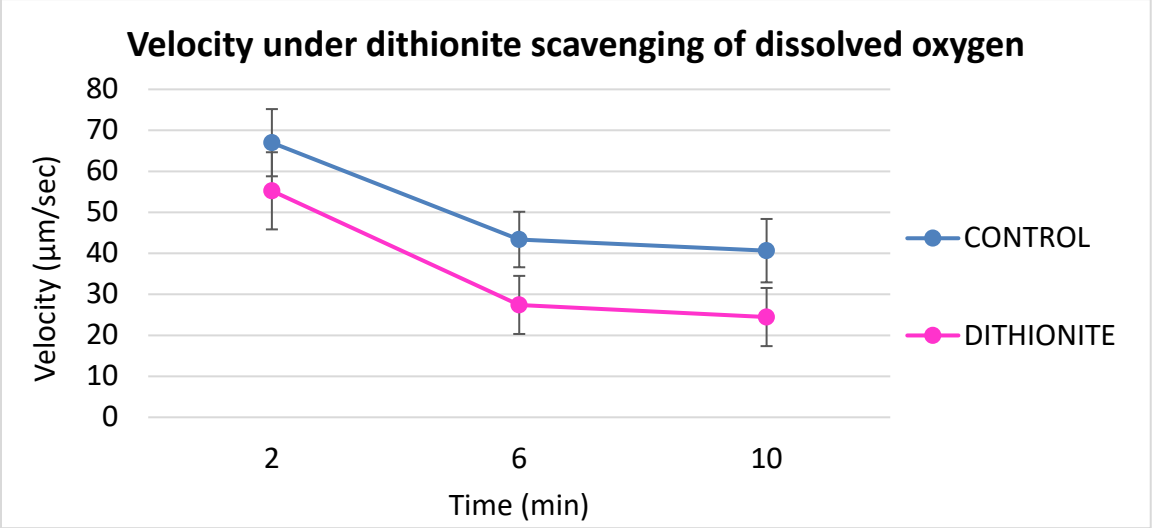

The presence of dithionite produced a slight but significant decrease in velocity at minutes 6 and 10 only ($p < 0.05$).

Figure 8g: Velocity under arginine kinase inhibition

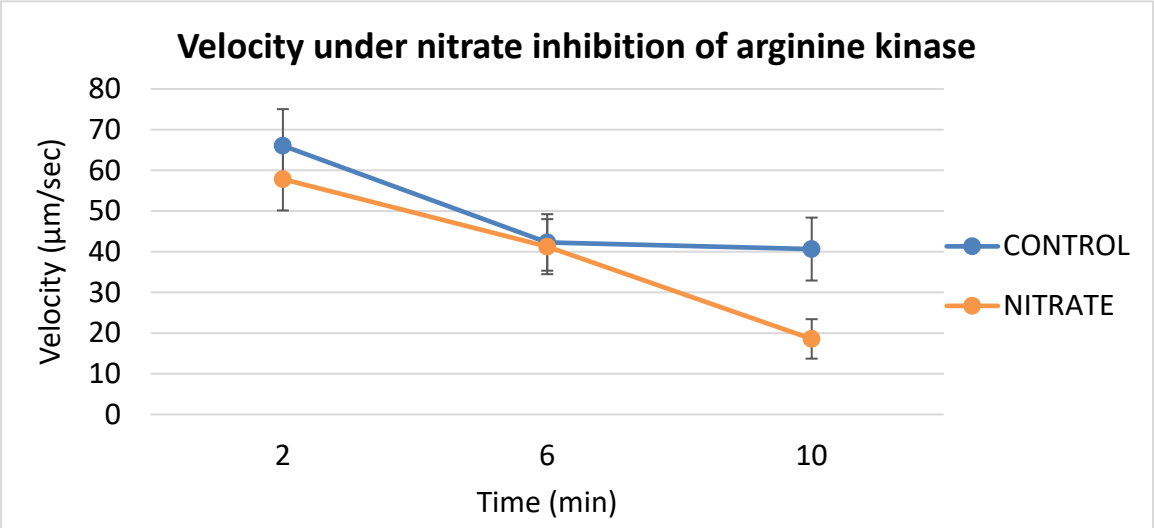

Nitrate significantly reduced velocity at 10 minutes ($p = 0.0005$).

Figure 9: Velocity under Orco activation

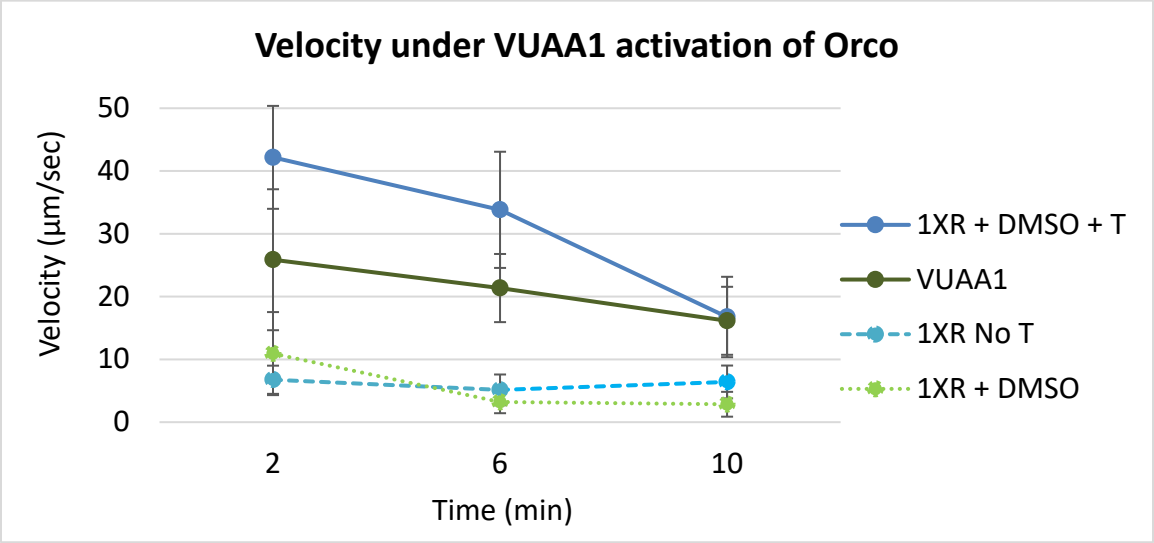

Orco activation by VUAA1 provides moderate activation of flagellar motility ($p < 0.05$).

Figure 10: Velocity under 8-Br-cAMP addition

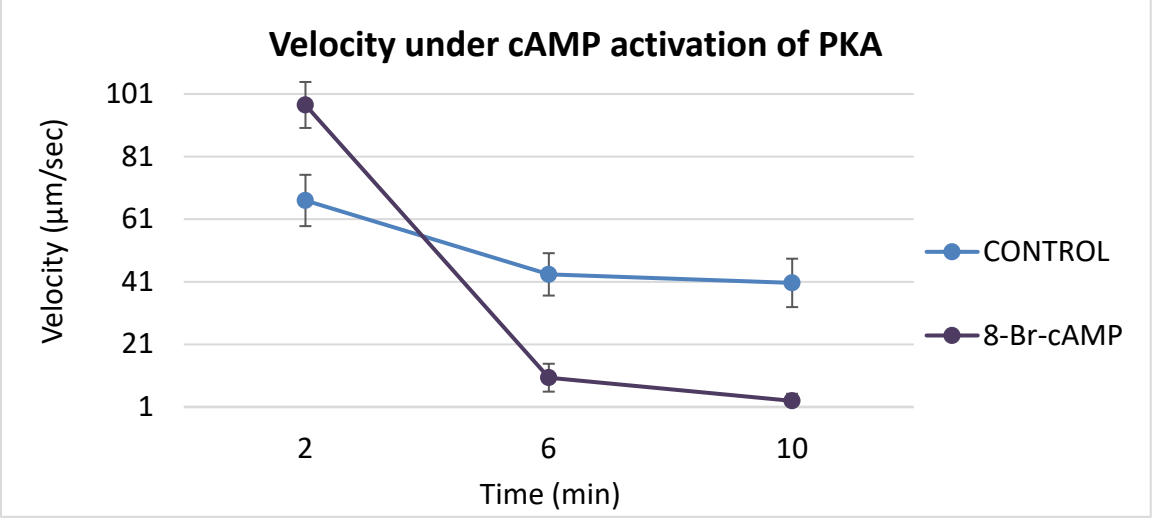

A membrane-permeable cAMP derivative activated motility significantly higher than the control at 2 minutes ($p = 0.0005$). This activity quickly ceased and velocity drastically reduced at 6 and 10 minutes.

Table 2: High relative abundance metabolic enzymes

Enzyme	P1	P2	P3
| CpipJ_CPIJ002029 | Arginine kinase	0.30	0.35	0.34
| CpipJ_CPIJ004776 | Glycogen phosphorylase	0.18	0.15	0.85
| CpipJ_CPIJ006209 | ATP synthase beta subunit	0.16	0.17	0.45

Relative abundances are reported for the three proteomes (P1, P2, and P3). Accession numbers are included above enzyme names. In P3, where peptide detection was the most sensitive, glycogen phosphorylase was seen to be 85% as abundant as structural proteins while ATP synthase's beta subunit was 45% as abundant and arginine kinase was 34% as abundant.

Data obtained from Thaler et. al. 2023[18]

Table 3: Relative abundances of anaerobic metabolic enzymes

Enzyme	P1	P2	P3
Glycolytic Enzymes			
| CpipJ_CPIJ008049 | Hexokinase (HK)	0.02	0.02	0.04
| CpipJ_CPIJ006486 | Phosphohexose Isomerase (PHI)	0.04	0.03	0.13
| CpipJ_CPIJ008591 | Phosphofructokinase 1 (PFK1)	0.00	0.00	0.05
| CpipJ_CPIJ009571 | Aldolase	0.08	0.08	0.25
| CpipJ_CPIJ002354 | Triose Phosphate Isomerase (TPI)	0.04	0.04	0.15
| CpipJ_CPIJ005597 | GAP Dehydrogenase (GAPDH)	0.06	0.04	0.29
| CpipJ_CPIJ009280 | Phosphoglycerate Kinase (PGK)	0.06	0.05	0.11
| CpipJ_CPIJ014577 | Phosphoglycerate mutase (PGM)	0.03	0.02	0.05
| CpipJ_CPIJ000948 | Enolase	0.12	0.09	0.19
| CpipJ_CPIJ008289 | Pyruvate Kinase (PK)	0.06	0.05	0.14
Fermentation Enzymes			
| CpipJ_CPIJ001318 | Lactate Dehydrogenase (LDH)	0.00	0.00	0.01
Pyruvate Decarboxylase (PD)	0.00	0.00	0.00
| CpipJ_CPIJ008783 | Alcohol Dehydrogenase (Alc-D)	0.00	0.00	0.04
| CpipJ_CPIJ007198 | Aldehyde Dehydrogenase (Ald-D)	0.01	0.02	0.09
Glycogenic Proteins and Enzymes			
| CpipJ_CPIJ013596 | Glycogenin	0.00	0.00	0.01
| CpipJ_CPIJ005681 | Phosphoglucomutase (PGM)	0.06	0.05	0.09
| CpipJ_CPIJ009610 | UDP-Glc Pyrophosphatase (UDPGP)	0.00	0.00	0.01
| CpipJ_CPIJ011898 | Pyrophosphatase	0.02	0.01	0.03
| CpipJ_CPIJ005086 | Glycogen Synthase (GS)	0.01	0.01	0.12
Branching Enzyme (BE)	0.00	0.00	0.00
| CpipJ_CPIJ013040 | Debranching Enzyme (DBE)	0.00	0.00	0.14
| CpipJ_CPIJ004776 | Glycogen Phosphorylase (GP)	0.18	0.15	0.85

Relative abundances of anaerobic metabolic enzymes found in the proteome and their accession numbers are provided.

Data obtained from Thaler et. al. 2023[18]

Table 4: Glycogen consumption

Condition	Final [Glycogen] (nM)	Glycogen Consumed (nM)
1XR	1.0	0.7
1XR+T	0.5	1.2
KCN-Glc+T	0.4	1.3

Table 4: Final glycogen concentrations are shown. Glycogen consumption is reported based on the difference between the CFR condition.

Table 5: Average velocities across conditions

Condition	2 Minutes	6 Minutes	10 Minutes
Positive Control	66.99 ± 8.20	43.37 ± 6.67	40.65 ± 7.73
Dithionite	55.25 ± 9.41	27.41 ± 7.09	24.46 ± 7.09
Glc-Free	49.79 ± 6.79	32.35 ± 5.58	22.53 ± 4.82
10 mM Citrate	27.50 ± 5.70	13.91 ± 4.13	17.43 ± 4.27
Nitrate	57.85 ± 7.70	37.01 ± 6.45	17.41 ± 4.58
1XR + DMSO + T	42.18 ± 8.20	33.82 ± 9.25	16.75 ± 6.41
VUAA1	25.87 ± 11.23	21.36 ± 5.42	16.15 ± 5.41
1XR	6.76 ± 4.17	5.14 ± 2.45	6.40 ± 2.62
5 nM GPI	21.32 ± 6.62	12.14 ± 5.19	4.32 ± 2.57
KCN	29.31 ± 5.57	9.88 ± 2.50	3.08 ± 1.33
8-Br-cAMP	97.51 ± 7.35	10.36 ± 4.46	2.95 ± 2.28
1XR + DMSO	10.92 ± 6.61	3.20 ± 1.78	2.85 ±1.98
KCN-Glc	23.36 ± 4.51	5.62 ± 2.10	2.32 ± 1.25
Negative Control	0	0	0

Average velocities are reported with standard error of the mean. Conditions are ranked according to velocity values at 10 minutes. Because the 5 and 10 mM citrate concentrations were not significantly different, only 10 mM citrate is reported. Similarly, because 5 nM GPI was found to be the most efficient concentration, all others were excluded.

Discussion

Significance

In 2022, over 76% of reported West Nile Virus cases in California led to neuroinvasive disease while 11% were fatal. Though total case numbers for these statistics were comparatively low (1035), the total number of cases from year to year has been documented to increase almost 8-fold.[1] Recent studies have demonstrated how climate change could increase the danger of this disease and others carried by mosquitoes[53]. With more frequent atmospheric rivers increasing the humidity and amount of standing water in California, it can be expected that mosquito populations will thrive. These disease vectors require water for several life stages[54] and prefer warm, humid environments[55]. Infected *Culex pipiens* females can cause illness in humans as well as livestock via blood transfer, but there is currently no prevention or treatment for these conditions[1]. Not only does this pose a risk to both populations from well-established viruses, but also provides an avenue for new zoonotic diseases to emerge.

An attractive method of arboviral disease reduction is population control of their vectors. The goal is not and should not be to entirely eradicate pest species, but to decrease population sizes. The disappearance of an entire species would surely disrupt ecosystems; therefore, any strategies employed in population decrease must have an intermediate efficacy such that extinction does not occur. The use of insecticides is a common approach to this aim. However, this chemical

tactic imparts negative human and ecological consequences as well as drives the evolution of insecticide-resistant strains. More recently, the scientific community has moved toward strategies that could circumvent such obstacles. Some of these techniques include induced cytoplasmic incompatibility using transinfected endosymbiont *Wolbachia pipientis*[2], entomopathogenic fungal infections[3], providing toxic food sources[4], and lethal or fertility-reducing genetic manipulations[5,6]. Reproductive success of a male is dependent upon the sperm's ability to penetrate an egg. This requires the activation of sperm from quiescence, a process involving both structural conformation changes as well as catabolic activation.

Proteomics

Due to the high energy demand of transcription and translation, it is expected that cells attenuate their proteomes to their specific needs to increase the efficiency of necessary functions. Therefore, proteins essential for cellular function, such as forward cellular velocity in sperm, are expected to have high relative abundances. It should be noted that the raw numbers reported in the proteomes do not represent copy numbers of a protein, rather the number of fragment hits associated with a known protein sequence. However, it can be expected that proteins with high relative abundances in the cell will also have more fragments detected in the experiment. Of course, very large proteins would also have slightly higher relative abundances, but not to the extent of proteins which are truly maintained at high concentrations. On the other hand, it is also

possible that proteins which are truly abundant in the cell were not detected at a level proportional to their concentrations due to chance. Similarly, some proteins may not be detected at all. Nonetheless, given the significance of many of the inhibition studies, the use of relative abundances was a good initial indicator of enzymes of interest.

The discovery of high relative abundances of glycogen phosphorylase, arginine kinase, and ATP synthase beta subunit (Table 2) suggests a story of its own. Either the mitochondria are functional early in development and the ATP synthase subunit is simply vestigial after maturation and mitochondrial paracrystallization, or the organelles remain at least partially functional as derivatives. Some invertebrate sperm store glycogen in granules within their flagella[15], potentially creating localized areas of increased ATP concentrations when glycogen's main catabolic product, glucose-6-phosphate (G6P), is eventually oxidized in glycolysis. This creates the need for a flux transfer chain like the creatine kinase system in human myocardial contractile cells whose activity inversely correlates with heart failure[19]. Due to the similarity of sarcomere and axoneme function, this suggests arginine kinase inhibition is a potential target for male *Culex* fertility reduction.

Glycogen Assays

The GPI used in this study was an allosteric inhibitor.[31] Glycogen assay results indicate it exhibits increased inhibition of glycogen consumption with increased concentrations (Figure 7b). The most robust inhibition of glycogen

consumption was seen with 200 nM GPI resulting in an average of 2 nM of glycogen remaining per cell. This value coincides well with the 1.7 nM of glycogen remaining when sperm are completely inhibited from motility in the CFR condition (Figure 7a). Additionally, the vehicle control (0 nM GPI) indicated 0.6 nM glycogen remained after activation while incubation in 1XR+T resulted in 0.5 nM glycogen remaining. It is noted that a higher consumption of glycogen is achieved when glucose is removed and the ETC is inhibited (Table 4).

Motility Assays

While forward cellular velocity is not a direct measurement of bioenergetics, the parameter serves as a useful proxy for ATP availability and consumption due to the understanding of the dynein motors' necessity for ATP in order to produce microtubule sliding. Therefore, the motility assays conducted in this study investigated the coupling of bioenergetics and biomechanics in *Culex* sperm. This is believed to be the first study of its kind.

The investigation of carbohydrate catabolism's role in forward cellular velocity was instructive. When glucose was removed from the extracellular space, a slight reduction in velocity was seen only at 10 minutes with respect to the control (Figure 8c). In contrast, successful inhibition of glycogen phosphorylase caused significant reduction in velocity and maintained an average below 10 μm/sec at all time points (Figure 8b). These results suggest glycogen breakdown is coupled with increased forward cellular velocity. While glucose from the extracellular space likely assists in maintaining a high glycolytic flux when

glycogen stores begin to deplete, it is the intracellular stores which most significantly contribute to ATP production for dynein use.

Interestingly, motility assay results did not show velocity to have an inverse relationship to GPI concentrations while glycogen consumption did (Figure 7b). Maximal velocity inhibition was seen at 5 and 50 nM while all other concentrations did not significantly reduce the cell's ability to swim with respect to control (Figure 8b). It is believed that this is the first study to have used this specific compound to inhibit glycogen phosphorylase in mosquito sperm. As such, there remains the possibility of unknown, confounding effects of the chemical on the cell's behavior.

Citrate inhibition of PFK1 successfully decreased velocity at each time point (Figure 8d). In either concentration, average velocity remains below 40 μm/sec throughout the experiment. These results suggest inhibition in this case is not complete, rather a downregulation in the activity of PFK1 has occurred. Here, trypsin is believed to have activated glycogen phosphorylase. Therefore, G6P is made available for glycolysis. However, if a reduction in the conversion of F6P to F1,6-bP results in a build-up of F6P, this will also result in a build-up of G6P due to the law of mass action (Figure 6a). At this point, although glycogen phosphorylase has been activated, the rate of its activity would likely reduce due to increasing concentrations of its product.

Results from the KCN and KCN-Glc conditions were of extreme interest. Because velocity was robustly reduced in both conditions with averages

remaining below 35 μm/sec at each time point, these data strongly suggest that oxidative phosphorylation is tightly coupled with forward cellular velocity. These data also indicate the paracrystalline mitochondrial derivatives do, indeed, retain ETC functionality. Not only is the function preserved, but it is essential for robust sperm activation. Because there was not a significant difference between the conditions with and without extracellular glucose, it appears *Culex* sperm specifically couple glycogen catabolism with oxidative phosphorylation. It is likely that NADH produced by GAPDH is oxidized at complex II of the ETC in order to increase the efficiency of G6P break down. The mechanism used by the cell to bring electrons from NADH into the mitochondria is still not known, but a shuttle mechanism is likely in place.

The KCN results, unfortunately, do not coincide well with the results from the dithionite condition (Figure 8f). It is expected that inhibition of the reduction of oxygen at the ETC would affect sperm in the same way an anoxic solution would. However, this discrepancy is likely due to the methods used across all motility assay conditions. While the concentration of dithionite used is effective in scavenging oxygen, the gas may dissolve and accumulate in solution upon dithionite saturation. Because motility assays were not completed in an anoxic chamber, it is likely that this occurred and only a hypoxic solution was achieved. Additionally, dithionite is very toxic to cells and may react with axonemal components resulting in altered swimming behavior on its own.

Another unexpected result was that of arginine kinase inhibition by nitrate. Significant reduction in velocity was only observed at minute 10, suggesting an arginine kinase ATP shuttle/regeneration system is only coupled to motility during late activation. It is possible that glycogen stores are spread well enough throughout the flagellum that a system is not required when an abundance of glycogen is available. However, after 10 minutes of robust activation, glycogen concentrations are expected to decrease. Perhaps it is only when ATP production begins to slow that a shuttle/regeneration system becomes necessary for the cell.

In addition to the investigation of energy production itself, this study sought to uncover signal transduction mechanisms utilized by the cell in order to activate catabolic pathways. Due to the known signaling mechanism involved in glycogen phosphorylase activation, a membrane-permeable cAMP derivative was used to activate protein kinase A (PKA). Extremely robust activation was induced at 2 minutes when 8-Br-cAMP was added to Ringer's. However, this activity ceased early on and subsequent velocity averages did not surpass 11 μm/sec. These results indicate activation of PKA is sufficient for robust motility activation in *Culex* sperm. However, due to the chemical instability of cAMP and presence of phosphodiesterase enzymes in the cell's proteome, it is likely that its concentration was very quickly reduced below levels capable of activating PKA, resulting in severely reduced motility at later time points.

This study has also confirmed in a double-blind fashion that calcium is necessary and sufficient for motility. In calcium-free Ringer's (CFR), sperm never

displayed any type of motility (Figure 8a) even in the presence of trypsin. Alternatively, in the absence of trypsin but presence of VUAA1, an activator for a channel known to permeate calcium (Orco), sperm attain moderate but significant forward cellular velocity (Figure 9). The significant difference between the VUAA1 condition and DMSO control at minutes 2 and 6 suggests that calcium alone is not sufficient for *robust* motility activation. These results coincide well with previous studies on *Culex* sperm demonstrating the necessity of calcium to initiate motility but of a MAPK phosphorylation event to increase velocity. This second step appears to be missing with Orco activation alone and suggest trypsin initiates a signal transduction cascade involving both the increase of intracellular calcium and the phosphorylation of signal transduction enzymes.

SpermQ

One obstacle encountered during data analysis via SpermQ was the requirement of sperm to remain in focus to obtain data meeting the kymograph quality threshold. Adequate freedom of depth was given to sperm to ensure flagella were not touching the glass, but this allowed cells to change the depths at which they were swimming during a recording. Thus, only a handful of sperm remained at optimal swimming depths throughout the recorded frames of interest and multiple trials (6-10) of the same condition were required to meet the desired number of cells to analyze per time point (27). Future studies could examine the minimum swimming depth required for sperm to swim freely and whether other CASA systems are better suited for *Culex* sperm.

Seahorse Analyzer

One method of interest not utilized for this study is a Seahorse Analyzer, capable of automating some of the inferences made here about the cell's metabolic activity. The machine directly measures baseline extracellular fluid acidity and oxygen concentration decrease around tethered cells in a well plate. Activators and inhibitors can then be added by the machine after the baseline measurement is complete. This early step was the crux holding *Culex* sperm back from analysis via Seahorse as they often spontaneously activate immediately upon release from the seminal vesicle (which would be required as a first step to tethering the cells to the well plate). In an attempt to overcome this obstacle, an experiment was conducted where sperm were incubated in CFR for 20 minutes and then calcium and trypsin were added simultaneously afterward to induce activation. However, attempts at producing motility similar to control conditions were not successful and motility assays were conducted, instead.

There are several considerations for future attempts of this experiment. These include the amount of calcium present in nanopure water and the sperm's intracellular space prior to activation (which is what necessitates the addition of EGTA to CFR). If these concentrations were known, EGTA saturation could be calculated. This is a slightly complicated task as the molecule also binds magnesium (a component of Ringer's). This was one potential source of error leading to failure of activation after CFR incubation. Another consideration is the effect of the incubation period on flagellar motility. If motility is altered, such

experiments could be used only to compare between groups and not as a measure of native flagellar behavior. Nonetheless, it would be a useful method in directly and precisely measuring sperm metabolism under various conditions.

Future Studies

While this study focused on glycolytic catabolism of glucose derivatives only, many insect sperm are known to take in fructose from the extracellular space for break down via glycolysis. Fructose has not yet been added to the Ringer's for this system and it would be of interest to know if one of the hexoses is preferred by the cell over the other.

One potentially interesting line of investigation is the fate of pyruvate in the cell to determine if it is mainly shunted into the citric acid cycle or if fermentation is also occurring to regenerate NAD^+ for glycolysis. Inhibition of NAD^+ regeneration could be an efficient mechanism by which to decrease sperm motility as glycolysis is necessary to achieve robust forward cellular velocity.

While the importance of ATP production for dynein power stroke activity cannot be understated, future studies should also investigate the extent of ATP hydrolysis for phosphorylation events at the axoneme. It would be of great interest to localize the components of the axoneme being phosphorylated as this modification could likely be inhibited. This mechanism could provide another avenue for attempts at *Culex* fertility reduction.

Fluorescence experiments will be conducted next to localize arginine kinase, glycogen phosphorylase, and active portions of the mitochondrial

membrane. The fluorescent indicator, MitoTracker, only fluoresces when introduced into extremely acidic environments such as the mitochondrial intermembrane space where the ETC is active. This dye then remains in place while further staining of arginine kinase and glycogen phosphorylase via fluorescently tagged antibodies is conducted.

Additionally, in order to test the full capacity of cAMP to activate *Culex* sperm, motility assays will be repeated with a phosphodiesterase inhibitor. Another interesting possibility is providing the sperm with a second dose of 8-Br-cAMP after motility has reduced. If motility is once again increased, this will strengthen the evidence that an increase in PKA activation causes increased velocity in the cell.

Conclusions

Trypsin likely interacts with some form of a protease activated receptor (PAR) resulting in G-protein subunit dissociation from their coupled receptor. This could activate an inward rectifying sodium channel and provide the membrane depolarization necessary for T-type voltage-gated calcium channels to open. Upon calcium influx, dynein is able to bind adjacent microtubules and soluble adenylyl cyclase activates to convert ATP to cAMP. PKA could then activate and induce ERK1/2 to phosphorylate axonemal components for increased forward cellular velocity. PKA also likely activates phosphorylase kinase which in turn activates glycogen phosphorylase. This enzyme reduces glycogen by one monomer which is readily converted to G6P. This product, along with any glucose entering the cell (presumably through a GLUT transporter) could then enter glycolysis to produce pyruvate, ATP, and NADH. Pyruvate's fate is not yet known, but lactic acid fermentation is likely for NAD^+ regeneration for glycolysis. The NADH is then further oxidized by the electron transport chain in order to increase the yield of ATP per carbohydrate monomer. An arginine kinase shuttle system could provide an avenue for ATP to travel to the axoneme and regenerate ATP directly at the site of the axoneme without the need of cellular respiration to supply hydrolytic energy for dynein's power stroke.

Figure 11: A proposed signal transduction pathway for aerobic glycogen catabolism

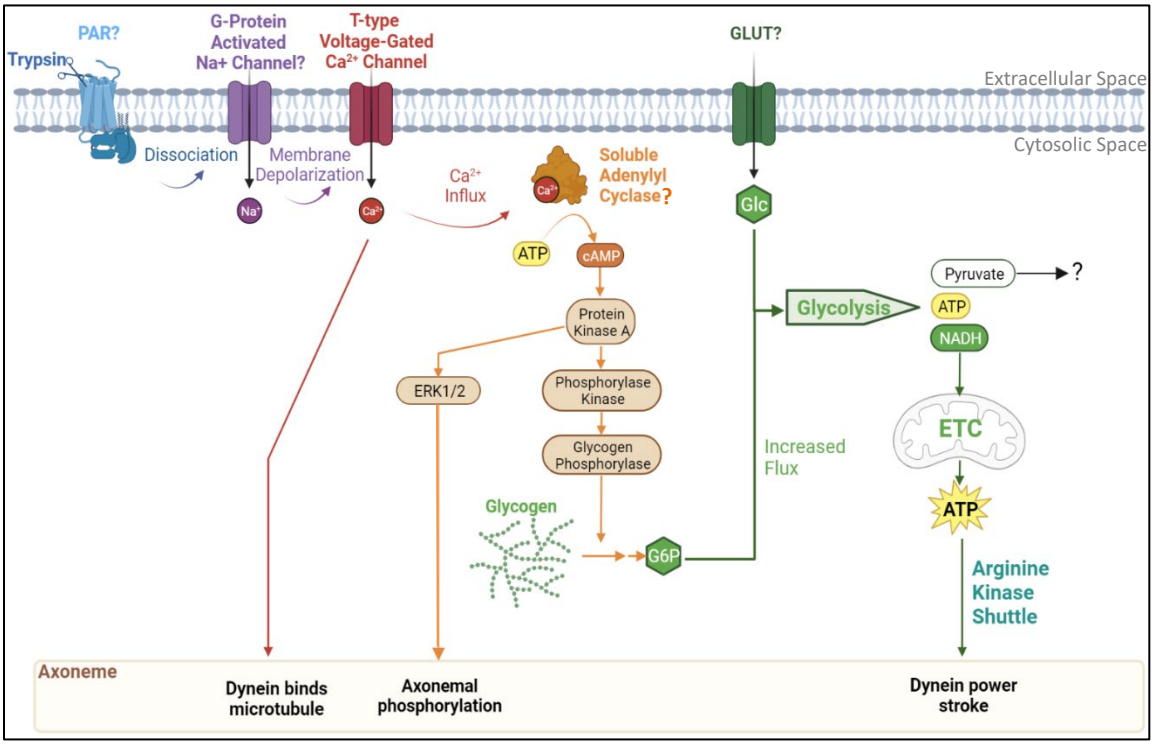

In consideration of all experimental results, a signal transduction pathway resulting in the mobilization of glycogen stores for increased glycolytic flux has been provided. There are several areas where hypotheses of proteins included are made based on experimental results and are indicated with a question mark. These proteins were not found in the proteome and are interesting topics for future studies.

References

1. West Nile Virus Disease Cases by State 2022. (2023). *Centers for Disease Control and Prevention.* https://www.cdc.gov/westnile/statsmaps/preliminarymapsdata2022/disease-cases-state-2022.html

2. Ant, T. H., Herd, C., Louis, F., Failloux, A. B., & Sinkins, S. P. (2020). Wolbachia transinfections in Culex quinquefasciatus generate cytoplasmic incompatibility. *Insect molecular biology*, *29*(1), 1–8. https://doi.org/10.1111/imb.12604

3. Ismail, H. M., Freed, S., Naeem, A., Malik, S., & Ali, N. (2020). The Effect of Entomopathogenic Fungi on Enzymatic Activity in Chlorpyrifos-Resistant Mosquitoes, Culex quinquefasciatus (Diptera: Culicidae). *Journal of medical entomology*, *57*(1), 204–213. https://doi.org/10.1093/jme/tjz143

4. Gu, Z. Y., He, J., Teng, X. D., Lan, C. J., Shen, R. X., Wang, Y. T., Zhang, N., Dong, Y. D., Zhao, T. Y., & Li, C. X. (2020). Efficacy of orally toxic sugar baits against contact-insecticide resistant culex quinquefasciatus. *Acta tropica*, *202*, 105256. https://doi.org/10.1016/j.actatropica.2019.105256

5. Williams, A. E., Franz, A. W. E., Reid, W. R., & Olson, K. E. (2020). Antiviral Effectors and Gene Drive Strategies for Mosquito Population Suppression or Replacement to Mitigate Arbovirus Transmission by *Aedes aegypti*. *Insects*, *11*(1), 52. https://doi.org/10.3390/insects11010052

6. Li, M., Li, T., Liu, N., Raban, R. R., Wang, X., & Akbari, O. S. (2020). Methods for the generation of heritable germline mutations in the disease vector Culex quinquefasciatus using clustered regularly interspaced short palindrome repeats-associated protein 9. *Insect molecular biology*, *29*(2), 214–220. https://doi.org/10.1111/imb.12626

7. Baccetti, B., Bruni, E., Gambera, L., Moretti, E., & Piomboni, P. (2004). An ultrastructural and immunocytochemical study of a rare genetic sperm tail defect that causes infertility in humans. *Fertility and sterility*, *82*(2), 463–468. https://doi.org/10.1016/j.fertnstert.2003.12.049

8. Baccetti, B., Burrini, A. G., & Pallini, V. (1980). Spermatozoa and cilia lacking axoneme in an infertile man. *Andrologia*, *12*(6), 525–532. https://doi.org/10.1111/j.1439-0272.1980.tb01344.x

9. Phillips D. M. (1969). Exceptions to the prevailing pattern of tubules (9 + 9 + 2) in the sperm flagella of certain insect species. *The Journal of cell biology*, *40*(1), 28–43. https://doi.org/10.1083/jcb.40.1.28

10. Phillips D. M. (1970). Insect sperm: their structure and morphogenesis. *The Journal of cell biology*, *44*(2), 243–277. https://doi.org/10.1083/jcb.44.2.243

11. Laurinyecz, B., Vedelek, V., Kovács, A. L., Szilasi, K., Lipinszki, Z., Slezák, C., Darula, Z., Juhász, G., & Sinka, R. (2019). Sperm-Leucylaminopeptidases are required for male fertility as structural components of mitochondrial paracrystalline material in Drosophila melanogaster sperm. *PLoS genetics*, *15*(2), e1007987. https://doi.org/10.1371/journal.pgen.1007987

12. Kamiya, R., & Yagi, T. (2014). Functional diversity of axonemal dyneins as assessed by in vitro and in vivo motility assays of Chlamydomonas mutants. *Zoological science*, *31*(10), 633–644. https://doi.org/10.2108/zs140066

13. Sakato, M., Sakakibara, H., & King, S. M. (2007). Chlamydomonas outer arm dynein alters conformation in response to Ca2+. *Molecular biology of the cell*, *18*(9), 3620–3634. https://doi.org/10.1091/mbc.e06-10-0917

14. Ford W. C. (2006). Glycolysis and sperm motility: does a spoonful of sugar help the flagellum go round?. *Human reproduction update*, *12*(3), 269–274. https://doi.org/10.1093/humupd/dmi053

15. Anderson, W. A., & Personne, P. (1970). The localization of glycogen in the spermatozoa of various invertebrate and vertebrate species. *The Journal of cell biology*, *44*(1), 29–51. https://doi.org/10.1083/jcb.44.1.29

16. Hansen, J. N., Rassmann, S., Jikeli, J. F., & Wachten, D. (2018). *SpermQ*-A Simple Analysis Software to Comprehensively Study Flagellar Beating and Sperm Steering. *Cells*, *8*(1), 10. https://doi.org/10.3390/cells8010010

17. Thaler, C. D., Miyata, H., Haimo, L. T., & Cardullo, R. A. (2013). Waveform generation is controlled by phosphorylation and swimming direction is controlled by Ca2+ in sperm from the mosquito Culex quinquefasciatus. *Biology of reproduction*, *89*(6), 135. https://doi.org/10.1095/biolreprod.113.109488

18. Thaler, C. D., Carstens, K., Martinez, G., Stephens, K., & Cardullo, R. A. (2023). Using the Culex pipiens sperm proteome to identify elements essential for mosquito reproduction. *PloS one*, *18*(2), e0280013. https://doi.org/10.1371/journal.pone.0280013

19. Bottomley, P. A., Panjrath, G. S., Lai, S., Hirsch, G. A., Wu, K., Najjar, S. S., Steinberg, A., Gerstenblith, G., & Weiss, R. G. (2013). Metabolic rates of ATP transfer through creatine kinase (CK Flux) predict clinical heart failure events and death. *Science translational medicine*, *5*(215), 215re3. https://doi.org/10.1126/scitranslmed.3007328

20. Pereira, R., Sá, R., Barros, A., & Sousa, M. (2017). Major regulatory mechanisms involved in sperm motility. *Asian journal of andrology*, *19*(1), 5–14. https://doi.org/10.4103/1008-682X.167716

21. Klabunde, T., Wendt, K. U., Kadereit, D., Brachvogel, V., Burger, H. J., Herling, A. W., Oikonomakos, N. G., Kosmopoulou, M. N., Schmoll, D., Sarubbi, E., von Roedern, E., Schönafinger, K., & Defossa, E. (2005). Acyl ureas as human liver glycogen phosphorylase inhibitors for the treatment of type 2 diabetes. *Journal of medicinal chemistry*, *48*(20), 6178–6193. https://doi.org/10.1021/jm049034y

22. Pitts, R. J., Liu, C., Zhou, X., Malpartida, J. C., & Zwiebel, L. J. (2014). Odorant receptor-mediated sperm activation in disease vector mosquitoes. *Proceedings of the National Academy of Sciences of the United States of America*, *111*(7), 2566–2571. https://doi.org/10.1073/pnas.1322923111

23. Martinez, Gabrielle. (2022). Calcium Homeostasis in the Activation and Regulation of Sperm Motility in the Culex Mosquito. *University of California Riverside, Doctoral Dissertation.*

24. Báo, S. N., & de Souza, W. (1994). Structural specialization in the flagellum of the spermatozoon of the bloodsucking bug (Rhodnius prolixus; Hemiptera, Reduviidae). *Tissue & cell*, *26*(3), 299–308. https://doi.org/10.1016/0040-8166(94)90016-7

25. Nigam, S. K., Bush, K. T., Martovetsky, G., Ahn, S. Y., Liu, H. C., Richard, E., Bhatnagar, V., & Wu, W. (2015). The organic anion transporter (OAT) family: a systems biology perspective. *Physiological reviews*, *95*(1), 83–123. https://doi.org/10.1152/physrev.00025.2013

26. Han, H. S., Kang, G., Kim, J. S., Choi, B. H., & Koo, S. H. (2016). Regulation of glucose metabolism from a liver-centric perspective. *Experimental & molecular medicine*, *48*(3), e218. https://doi.org/10.1038/emm.2015.122

27. Köttgen, M., Hofherr, A., Li, W., Chu, K., Cook, S., Montell, C., & Watnick, T. (2011). Drosophila sperm swim backwards in the female reproductive tract and are activated via TRPP2 ion channels. *PloS one*, *6*(5), e20031. https://doi.org/10.1371/journal.pone.0020031

28. Gray, J. (1995). The Movement of Sea-Urchin Spermatozoa. *Journal of Experimental Biology,* 32(4), 775–801. doi: https://doi.org/10.1242/jeb.32.4.775

29. Lattao, R., Bonaccorsi, S., & Gatti, M. (2012). Giant meiotic spindles in males from Drosophila species with giant sperm tails. *Journal of cell science*, *125*(Pt 3), 584–588. https://doi.org/10.1242/jcs.101469

30. Gu, N. H., Zhao, W. L., Wang, G. S., & Sun, F. (2019). Comparative analysis of mammalian sperm ultrastructure reveals relationships between sperm morphology, mitochondrial functions and motility. *Reproductive biology and endocrinology: RB&E*, *17*(1), 66. https://doi.org/10.1186/s12958-019-0510-y

31. Miyata, H., Morohoshi, A., & Ikawa, M. (2020). Analysis of the sperm flagellar axoneme using gene-modified mice. *Experimental animals*, *69*(4), 374–381. https://doi.org/10.1538/expanim.20-0064

32. Reck-Peterson, S. L., Redwine, W. B., Vale, R. D., & Carter, A. P. (2018). The cytoplasmic dynein transport machinery and its many cargoes. *Nature reviews. Molecular cell biology*, *19*(6), 382–398. https://doi.org/10.1038/s41580-018-0004-3

33. Ishikawa T. (2012). Structural biology of cytoplasmic and axonemal dyneins. *Journal of structural biology*, *179*(2), 229–234. https://doi.org/10.1016/j.jsb.2012.05.016

34. Tokuyasu K. T. (1975). Dynamics of spermiogenesis in Drosophila melanogaster. VI. Significance of "onion" nebenkern formation. *Journal of ultrastructure research*, *53*(1), 93–112. https://doi.org/10.1016/s0022-5320(75)80089-x

35. Perotti M. E. (1973). The mitochondrial derivative of the spermatozoon of Drosophila before and after fertilization. *Journal of ultrastructure research*, *44*(3), 181–198. https://doi.org/10.1016/s0022-5320(73)80055-3

36. Kubo, S., & Bui, K. H. (2023). Regulatory mechanisms of the dynein-2 motility by post-translational modification revealed by MD simulation. *Scientific reports*, *13*(1), 1477. https://doi.org/10.1038/s41598-023-28026-z

37. Gadadhar, S., Alvarez Viar, G., Hansen, J. N., Gong, A., Kostarev, A., Ialy-Radio, C., Leboucher, S., Whitfield, M., Ziyyat, A., Touré, A., Alvarez, L., Pigino, G., & Janke, C. (2021). Tubulin glycylation controls axonemal dynein activity, flagellar beat, and male fertility. *Science (New York, N.Y.)*, *371*(6525), pii: eabd4914. doi: 10.1126/science.abd4914. https://doi.org/10.1126/science.abd4914

38. Ikegami, K., & Setou, M. (2010). Unique post-translational modifications in specialized microtubule architecture. *Cell structure and function*, *35*(1), 15–22. https://doi.org/10.1247/csf.09027

39. Cai, X., & Clapham, D. E. (2008). Evolutionary genomics reveals lineage-specific gene loss and rapid evolution of a sperm-specific ion channel complex: CatSpers and CatSperbeta. *PloS one*, *3*(10), e3569. https://doi.org/10.1371/journal.pone.0003569

40. Longo F. J. (1973). Fertilization: a comparative ultrastructural review. *Biology of reproduction*, *9*(2), 149–215. https://doi.org/10.1093/biolreprod/9.2.149

41. Wachten, D., Jikeli, J. F., & Kaupp, U. B. (2017). Sperm Sensory Signaling. *Cold Spring Harbor perspectives in biology*, *9*(7), a028225. https://doi.org/10.1101/cshperspect.a028225

42. Miyata, H., Thaler, C. D., Haimo, L. T., & Cardullo, R. A. (2012). Protease activation and the signal transduction pathway regulating motility in sperm from the water strider Aquarius remigis. *Cytoskeleton (Hoboken, N.J.)*, *69*(4), 207–220. https://doi.org/10.1002/cm.21012

43. Xu, X., Wang, Y., Chen, J., Du, X., Yao, L., Xu, J., Zhang, Y., Huang, Y., & Wang, Y. (2022). Mutation of *Serine protease 1* Induces Male Sterility in *Bombyx mori*. *Frontiers in physiology*, *13*, 828859. https://doi.org/10.3389/fphys.2022.828859

44. Bi, H., Xu, X., Li, X., Wang, Y., Zhou, S., & Huang, Y. (2022). CRISPR/Cas9-mediated *Serine protease 2* disruption induces male sterility in *Spodoptera litura*. *Frontiers in physiology*, *13*, 931824. https://doi.org/10.3389/fphys.2022.931824

45. Matsuzaki, M., Mizushima, S., Hiyama, G., Hirohashi, N., Shiba, K., Inaba, K., Suzuki, T., Dohra, H., Ohnishi, T., Sato, Y., Kohsaka, T., Ichikawa, Y., Atsumi, Y., Yoshimura, T., & Sasanami, T. (2015). Lactic acid is a sperm motility inactivation factor in the sperm storage tubules. *Scientific reports*, *5*, 17643. https://doi.org/10.1038/srep17643

46. Kumar, L., Yadav, S. K., Kushwaha, B., Pandey, A., Sharma, V., Verma, V., Maikhuri, J. P., Rajender, S., Sharma, V. L., & Gupta, G. (2016). Energy Utilization for Survival and Fertilization-Parsimonious Quiescent Sperm Turn Extravagant on Motility Activation in Rat. *Biology of reproduction*, *94*(4), 96. https://doi.org/10.1095/biolreprod.115.137752

47. Gibbons, B. H., & Gibbons, I. R. (1980). Calcium-induced quiescence in reactivated sea urchin sperm. *The Journal of cell biology*, *84*(1), 13–27. https://doi.org/10.1083/jcb.84.1.13

48. Aitken R. J. (2000). Possible redox regulation of sperm motility activation. *Journal of andrology*, *21*(4), 491–496.

49. Usselman, M. C., & Cone, R. A. (1983). Rat sperm are mechanically immobilized in the caudal epididymis by "immobilin," a high molecular weight glycoprotein. *Biology of reproduction*, *29*(5), 1241–1253. https://doi.org/10.1095/biolreprod29.5.1241

50. Elgeti, J., Winkler, R. G., & Gompper, G. (2015). Physics of microswimmers--single particle motion and collective behavior: a review. *Reports on progress in physics. Physical Society (Great Britain)*, *78*(5), 056601. https://doi.org/10.1088/0034-4885/78/5/056601

51. Breitbart, H., & Spungin, B. (1997). The biochemistry of the acrosome reaction. *Molecular human reproduction*, *3*(3), 195–202. https://doi.org/10.1093/molehr/3.3.195

52. Wilson, K. L., Fitch, K. R., Bafus, B. T., & Wakimoto, B. T. (2006). Sperm plasma membrane breakdown during Drosophila fertilization requires sneaky, an acrosomal membrane protein. *Development (Cambridge, England)*, *133*(24), 4871–4879. https://doi.org/10.1242/dev.02671

53. Thomson, M. C., & Stanberry, L. R. (2022). Climate Change and Vectorborne Diseases. *The New England journal of medicine*, *387*(21), 1969–1978. https://doi.org/10.1056/NEJMra2200092

54. Mosquito Life Cycles. (2022). *Centers for Disease Control and Prevention*. https://www.cdc.gov/mosquitoes/about/life-cycles/index.html

55. Drakou, K., Nikolaou, T., Vasquez, M., Petric, D., Michaelakis, A., Kapranas, A., Papatheodoulou, A., & Koliou, M. (2020). The Effect of Weather Variables on Mosquito Activity: A Snapshot of the Main Point of Entry of Cyprus. *International journal of environmental research and public health*, *17*(4), 1403. https://doi.org/10.3390/ijerph17041403

56. Brown, A. E., & Grossman, S. H. (2004). The mechanism and modes of inhibition of arginine kinase from the cockroach (Periplaneta americana). *Archives of insect biochemistry and physiology*, *57*(4), 166–177. https://doi.org/10.1002/arch.20026

57. Newsholme, E. A., Sugden, P. H., & Williams, T. (1977). Effect of citrate on the activities of 6-phosphofructokinase from nervous and muscle tissues from different animals and its relationships to the regulation of glycolysis. *The Biochemical journal*, *166*(1), 123–129. https://doi.org/10.1042/bj1660123

58. SALAS, M. L., VINUELA, E., SALAS, M., & SOLS, A. (1965). CITRATE INHIBITION OF PHOSPHOFRUCTOKINASE AND THE PASTEUR EFFECT. *Biochemical and biophysical research communications*, *19*, 371–376. https://doi.org/10.1016/0006-291x(65)90471-7